Negative-temperature-state relaxation and reservoir-assisted quantum entanglement in double-spin-domain systems

Yusuke Hama,[1,*] Emi Yukawa,[2] William J. Munro,[1,3] and Kae Nemoto[1]
[1]*National Institute of Informatics, 2-1-2 Hitotsubashi, Chiyoda-ku, Tokyo 101-8430, Japan*
[2]*RIKEN Center for Emergent Matter Science (CEMS), Wako, Saitama 351-0198, Japan*
[3]*NTT Basic Research Laboratories and Research Center for Theoretical Quantum Physics, NTT Corporation, 3-1 Morinosato-Wakamiya, Atsugi-shi, Kanagawa 243-0198, Japan*

(Received 27 April 2018; published 27 November 2018)

Spin collective phenomena including superradiance are even today being intensively investigated with experimental tests performed based on state-of-the-art quantum technologies. Such attempts are not only for the simple experimental verification of predictions from the last century, but also as a motivation to explore new applications of spin collective phenomena and the coherent control of the coupling between spin ensembles and reservoirs. In this paper, we investigate the open quantum dynamics of two spin ensembles (double-spin domains) coupled to a common bosonic reservoir. We analyze in detail the dynamics of our collective state and its structure by focusing on both the symmetry and asymmetry of this coupled spin system. We find that when the spin size of one of the double domains is larger than that of the other domain, at the steady state this system exhibits two unusual collective behaviors: the negative-temperature-state relaxation in the smaller spin domain and the reservoir-assisted quantum entanglement between the two domains. These results are the consequence of the asymmetry of this system and the decoherence driven by the common reservoir.

DOI: 10.1103/PhysRevA.98.052133

I. INTRODUCTION

Our recent advances in material device fabrication as well as highly effective signal detection have allowed us to reach the stage where various Gedanken experiments from the earlier stages of quantum physics can be realized in the laboratory. (These include, for instance, quantum interference using a double slit, Bose-Einstein condensation, and superradiance [1–3].) We are now entering at the era where we can integrate multiple subquantum systems together into a single multifunctional quantum system [hybrid quantum systems, for instance, atoms coupled to optical cavities and nitrogen-vacancy (NV) centers in diamond coupled to flux qubit in superconducting circuits] [4–6]. The engineering of the hybrid quantum systems has been performed in quite diverse systems using elements coming from condensed matter to atomic, molecular, and optical systems [4–17]. Such a multifunctionality of these hybrid quantum systems is superior to the functionalities of any individual systems [4–7,18]. These developments have paved the way to allow us to explore novel phenomena in many-body and nonequilibrium quantum physics inherent from the hybridization process. Further, they may allow new techniques for performing the quantum information processing.

One of the major focuses in hybrid quantum physics is the exploration of collective phenomena motivated by spin ensembles being coherently or collectively coupled to bosonic modes [4–7,19,20]. When a spin ensemble couples collectively to bosons, it shows stronger coupling than that between individual spin and bosons, which scales with the square root of the total spin number [4–7,19–21]. The dynamics are characterized by this spin number N (the size of spin ensemble) and are generally very different from the single-spin dynamics. The typical example is the superradiance, where the spin ensemble shows extremely rapid decay on a timescale of $1/N$ with the strong radiative intensity also scaling with N^2 [3,22,23]. Although it was proposed by Dicke over 60 years ago [3], superradiance and such collective quantum phenomena remain as both fascinating and important research fields in various systems using the state-of-the-art quantum technologies, such as cavity quantum electrodynamic systems with atomic, molecular, and optical setups [13] and solids [23].

Most prior research in superradiance has, however, focused on this collective phenomena with a single spin ensemble. We are now able to design and fabricate devices with multiple ensembles present on them. The next step is to analyze collective phenomena generated by the multiple spin ensembles and explore ways to control the coupling structure between multiple spin ensembles and the reservoirs. Such investigations will be important and interesting for two reasons. First and foremost since the dynamics of a single spin and those of the collective spin are radically different as in the case of the superradiance, we expect the nontrivial dynamics of multiple spin ensembles to arise owing to its complicated structure. Second, collective spins form a strong coupling between bosons. The creation of this collective-spin-induced strong coupling as well as engineering of quantum reservoirs are going to be important ingredients for quantum information processing [4–7,19–21,24,25]. The novel spin collective phenomena are starting to emerge in various experimental setups focused on coherently controlling multiple spin ensembles and the reservoir [29–33].

*yskhama@nii.ac.jp

Towards these goals, we investigate in this paper the dynamics of the system with two spin ensembles (double-spin domains, for instance, double-nuclear-spin domains in GaAs semiconductors [26–28,34] and electron-spin ensembles in NV centers in diamond [32,33]) coupled to a common bosonic reservoir. We begin by examining what kind of collective phenomena and its associated steady state are induced by the common bosonic reservoir characterizing them by the two spin-ensemble (domain) sizes (the numbers of spins present in each of the domains). When the first spin-domain size is much larger than the second, the double-spin domains relax to steady states exhibiting two features: First is that the small spin domain relaxes to the negative-temperature state where the average excited-state population is greater than 50% [35]. Second is the creation of quantum entanglement between the two domains (even though they are not directly coupled together). These phenomena are realized due to the asymmetry of the double-spin domains and decoherence driven by the common reservoir.

This paper is organized as follows. It begins in Sec. II with our mathematical model of the double-spin domains coupled to the common bosonic reservoir. Then in Sec. III (which presents the main results of this paper) we discuss how to analyze the dynamics of our double-spin-domain system and its structure using a symmetry argument. In particular, we will investigate the steady state characterized by the sizes of two spin ensembles. We present two collective phenomena intrinsic to this system: the negative-temperature-state relaxation of the smaller domain and reservoir-assisted quantum entanglement generated between the spin domains. In Sec. IV, we discuss how to realize these two collective spin phenomena by presenting two candidate hybrid quantum systems. In Sec. V, we present a generalization of the previous argument for larger spin systems. Finally in Sec. VI we give a concluding discussion of this paper.

II. MODELING

In this section, we present a mathematical model of our double-spin-domain system. As shown in Fig. 1, it is a hybrid quantum system consisting of two spin ensembles coupled to a common bosonic reservoir R, each with a coupling constant g. The temperature of the reservoir is T. Now let us name the first (second) domain as $D_{\mathrm{A(B)}}$. The domain $D_{\mathrm{A(B)}}$ includes $N_{\mathrm{A(B)}}$ individual spin-1/2 particles. All the spins in the double domain are identical species. The spin frequency is given by ω_{s}. Due to these conditions, both spin ensembles in the domains D_{A} and D_{B} couple to the common reservoir R collectively, and these two spin ensembles act as collective spins $J_{\mathrm{A}}^{\alpha}=\sum_{i_{\mathrm{A}}=1}^{N_{\mathrm{A}}} S_{i_{\mathrm{A}}}^{\alpha}$ and $J_{\mathrm{B}}^{\alpha}=\sum_{i_{\mathrm{B}}=N_{\mathrm{A}}+1}^{N_{\mathrm{A}}+N_{\mathrm{B}}} S_{i_{\mathrm{B}}}^{\alpha}$. Here J_a^{α} ($\alpha=x,y,z.$) are the collective spin operators for x,y,z components of the domain a ($a=\mathrm{A},\mathrm{B}$) whose spin sizes are $N_{\mathrm{A}}/2$ and $N_{\mathrm{B}}/2$, respectively. $S_{i_{\mathrm{A}}}^{\alpha}$ ($S_{i_{\mathrm{B}}}^{\alpha}$) is the i_{A}th (i_{B}th) 1/2-spin operator. Our combined system is described by the Hamiltonian

$$H=\hbar\omega_{\mathrm{s}}\left(J_{\mathrm{A}}^{z}+J_{\mathrm{B}}^{z}\right)+\int d^{d}k\; E_{\boldsymbol{k}} r_{\boldsymbol{k}}^{\dagger} r_{\boldsymbol{k}} + \frac{\hbar g}{2}[(J_{\mathrm{A}}^{+}+J_{\mathrm{B}}^{+})R+(J_{\mathrm{A}}^{-}+J_{\mathrm{B}}^{-})R^{\dagger}]. \tag{1}$$

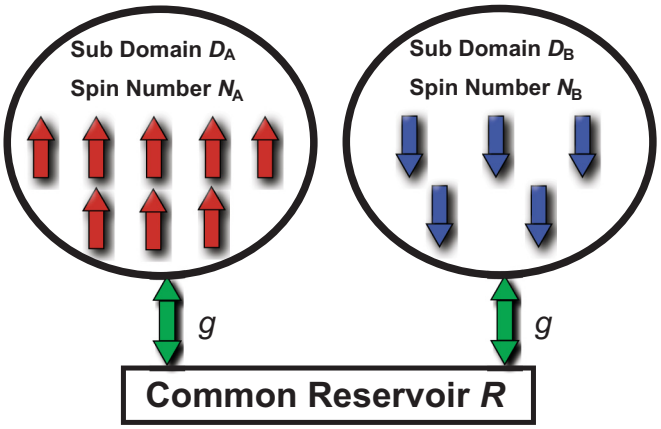

FIG. 1. The illustration of a double-spin-domain system consists of two one-half-spin ensembles and a common bosonic reservoir. The two spin domains couple equivalently to the common reservoir with a constant g represented by two green arrows. The first domain D_{A} has N_{A} spins indicated by up red arrows, whereas the second domain D_{B} contains N_{B} spins described by blue arrows. All the spins are identical.

The first and second terms represent the Hamiltonian of the two spin domains and the common reservior R, respectively. The spin operators $J_a^{\pm}=J_a^{x}\pm i J_a^{y}$ are the rising and lowering operators of domain a. $E_{\boldsymbol{k}}$ is the dispersion relation with $\boldsymbol{k}$, its wave vector. We will take $E_{\boldsymbol{k}}$ to be linear. The dimension d is the spatial dimension of this system, while $r_{\boldsymbol{k}}$ and $r_{\boldsymbol{k}}^{\dagger}$ are annihilation and creation operators of the reservoir, respectively. They satisfy the commutation relation $[r_{\boldsymbol{k}}, r_{\boldsymbol{k}'}^{\dagger}]=\delta(\boldsymbol{k}-\boldsymbol{k}')$. The third term represents the interaction between the two spin domains and the common reservoir. $R=\int d^{d}k\kappa_{\boldsymbol{k}} r_{\boldsymbol{k}}$ is the reservoir operator described by the annihilation operator $r_{\boldsymbol{k}}$ with a continuous function $\kappa_{\boldsymbol{k}}$. The formula of $\kappa_{\boldsymbol{k}}$ is determined by the system we are considering.

The dynamics we will analyze is the relaxation processes of the double-spin domain induced by the reservoir R. Such processes are described by the Lindblad master equation in the interaction picture as [36]

$$\dot{\rho}(t)=\gamma[(\bar{n}+1)\mathcal{L}(J_{\mathrm{A}}^{-}+J_{\mathrm{B}}^{-})+\bar{n}\mathcal{L}(J_{\mathrm{A}}^{+}+J_{\mathrm{B}}^{+})]\rho(t), \tag{2}$$

where the dot "·" represents the time derivative and the Born-Markov approximation has been applied. The reduced density matrix ρ is defined by tracing out the reservoir degrees of freedom over the total density matrix as $\rho(t)=\mathrm{Tr}_{\mathrm{R}}[\rho_{\mathrm{tot}}(t)]$. The reservoir density matrix is given by $\rho_{\mathrm{R}}=\exp(-H_{\mathrm{R}}/k_{\mathrm{B}}T)/\mathrm{Tr}_{\mathrm{R}}[\exp(-H_{\mathrm{R}}/k_{\mathrm{B}}T)]$, where H_{R} is the second term in the total Hamiltonian (1) with k_{B} the Boltzmann constant. The superoperator $\mathcal{L}(X)$ is defined by $\mathcal{L}(X)=2X\rho X^{\dagger}-X^{\dagger}X\rho-\rho X^{\dagger}X$, whereas γ is the damping rate described by the coupling g and $|\kappa_{\boldsymbol{k}}|^2$ at the wave vector $\boldsymbol{k}_{\mathrm{s}}$, which satisfies $E_{\boldsymbol{k}_{\mathrm{s}}}=\hbar\omega_{\mathrm{s}}$. $\bar{n}=1/(e^{\hbar\omega_{\mathrm{s}}/k_{\mathrm{b}}T}-1)$ is the Bose-Einstein distribution for the bosonic reservoir at energy $\hbar\omega_{\mathrm{s}}$. The first term in Eq. (2) describes the emission process of the spin ensembles while the second term represents the absorption process. In the following, we will solve the master equation at $T=0$ ($\bar{n}=0$). For an initial state, we examine the

antiparallel configuration

$$|\mathrm{is}\rangle = |\uparrow \ldots \uparrow\rangle_{\mathrm{A}} \otimes |\downarrow \ldots \downarrow\rangle_{\mathrm{B}}. \tag{3}$$

Here we choose the up (down)-spin state to be the excited (ground) state. The spin numbers are chosen such that $N_{\mathrm{A}} \geqslant N_{\mathrm{B}}$. The relaxation processes in the double-spin-domain system are mathematically described by two expectation values, $\langle J_{\mathrm{A}}\rangle = \mathrm{Tr}(\rho J_{\mathrm{A}})$ and $\langle J_{\mathrm{B}}\rangle = Tr(\rho J_{\mathrm{B}})$. All the dynamics we consider in this paper start with the initial state (3). As we will see, the relaxation processes are the collective phenomena described by the two spin sizes N_{A} and N_{B}.

III. SYSTEM STRUCTURE

In this section, we will present the dynamics and the structure of the reduced density matrix ρ for the double-spin domain (3) via the master equation (2). In particular, we will analyze in detail the structure of the steady state characterized by the two spin sizes. For a preparation, we will first introduce a tensor-product spin space, a direct-sum spin space, and then explain their relations. We will solve the master equation (2) in the direct-sum spin space and derive the steady-state solution. Then by switching from the direct-sum spin space to the tensor-product spin space, we will analyze the spin population (polarization) in each domain and the quantum entanglement between the two domains.

A. Tensor-product and direct-sum spin subspaces

At the initial time, the double-domain system under consideration has a structure represented by Eq. (3), i.e., $|\mathrm{is}\rangle = |\uparrow \ldots \uparrow\rangle_{\mathrm{A}} \otimes |\downarrow \ldots \downarrow\rangle_{\mathrm{B}}$. The initial state (3) is fully symmetric in each domain but is not in the total spin system $D = D_{\mathrm{A}} + D_{\mathrm{B}}$. Here we mean the symmetric state as a state which is fully invariant under the permutation between any two spins.

The total Hamiltonian (1) is described by the total spin $J^{\alpha} = J^{\alpha}_{\mathrm{A}} + J^{\alpha}_{\mathrm{B}}$ and satisfies $[\boldsymbol{J}^2, H] = [(J^x)^2 + (J^y)^2 + (J^z)^2, H] = 0$, which means that the total spin angular momentum is conserved and $[\boldsymbol{J}^2_{\mathrm{A(B)}}, H] = [(J^x_{\mathrm{A(B)}})^2 + (J^y_{\mathrm{A(B)}})^2 + (J^z_{\mathrm{A(B)}})^2, H] = 0$, implying the conservation of the angular moment of each spin domain. These conditions constrain the dynamics of the system. To capture this, we employ the direct-sum spin state representation. This allows us to largely reduce the Hilbert space to analyze the dynamics. Then, later we transform the state of interest to the composite picture (tensor-product representation) to evaluate the entanglement between the domains. In the direct-sum representation, we can easily identify which subspaces are relevant to the system dynamics. The mechanism of the collective relaxation in this system then becomes clearly understood and the steady-state formula is simply calculated.

In preparation for spin state analysis, let us introduce the above two spin spaces and explain their relations. First, the total spin space is given by

$$V_{\mathrm{tot}} = \mathcal{H}_{\mathrm{A}} \otimes \mathcal{H}_{\mathrm{B}}, \tag{4}$$

where $\mathcal{H}_{\mathrm{A}}$ and $\mathcal{H}_{\mathrm{B}}$ are spin subspaces whose dimensions are $2^{N_{\mathrm{A}}}$ and $2^{N_{\mathrm{B}}}$, respectively, giving the total dimension of $2^{N_{\mathrm{A}}+N_{\mathrm{B}}}$ for V_{tot}. From the spin-angular-momentum conservation $[\boldsymbol{J}^2_{\mathrm{A(B)}}, H] = 0$ and the symmetry of the initial state (3), the Hilbert space which describes the system dynamics is highly reduced from the full space V_{tot}. We will call it V_{rel}, and next, let us analyze its structure. We introduce the two subspaces $V^{\mathrm{sym}}_{\mathrm{A}}$ and $V^{\mathrm{sym}}_{\mathrm{B}}$, which are symmetric with respect to $\boldsymbol{J}_{\mathrm{A}}$ and $\boldsymbol{J}_{\mathrm{B}}$, respectively. The subspace $V^{\mathrm{sym}}_{\mathrm{A(B)}}$ is spanned by the eigenstates $|m_{\mathrm{A(B)}}\rangle_{\mathrm{A(B)}}$ which satisfy $\boldsymbol{J}^2_{\mathrm{A(B)}}|m_{\mathrm{A(B)}}\rangle_{\mathrm{A(B)}} = j_{\mathrm{A(B)}}(j_{\mathrm{A(B)}}+1)|m_{\mathrm{A(B)}}\rangle_{\mathrm{A(B)}}$ and $J^z_{\mathrm{A(B)}}|m_{\mathrm{A(B)}}\rangle_{\mathrm{A(B)}} = m_{\mathrm{A(B)}}|m_{\mathrm{A(B)}}\rangle_{\mathrm{A(B)}}$. Here $j_{\mathrm{A(B)}} = N_{\mathrm{A(B)}}/2$ and $m_{\mathrm{A(B)}} = j_{\mathrm{A(B)}}, j_{\mathrm{A(B)}} - 1, \ldots, -j_{\mathrm{A(B)}}$ are quantum numbers. The initial state (3) is described in the form $|m_{\mathrm{A}}\rangle_{\mathrm{A}} \otimes |m_{\mathrm{B}}\rangle_{\mathrm{B}}$, which are the basis vectors of the tensor-product subspace $V^{\mathrm{sym}}_{\mathrm{A}} \otimes V^{\mathrm{sym}}_{\mathrm{B}}$. On the other hand, the total Hamiltonian (1) or the Lindblad operator in Eq. (2) is described by the total spin operator J^{α}. This means that the initial state (3) decays by the total spin operator and the spin state is described in terms of the states in $V^{\mathrm{sym}}_{\mathrm{A}} \otimes V^{\mathrm{sym}}_{\mathrm{B}}$ for arbitrary time. Therefore, the subspace V_{rel} is identified with $V^{\mathrm{sym}}_{\mathrm{A}} \otimes V^{\mathrm{sym}}_{\mathrm{B}}$. Furthermore, the spin domain $D_{\mathrm{A(B)}}$ behaves as a collective spin $J_{\mathrm{A(B)}}$ whose spin size is equal to $N_{\mathrm{A(B)}}/2$ owing to this Hilbert-space identification. The dimension of the subspace V_{rel} is $(N_{\mathrm{A}}+1)(N_{\mathrm{B}}+1)$, which is sufficiently smaller than that of V_{tot}. The focus on V_{rel} makes the analysis of the system dynamics simple and effective.

Now we convert the V_{rel} to the direct-sum representation by the spin-angular-momentum composition of $\boldsymbol{J}_{\mathrm{A}}$ and $\boldsymbol{J}_{\mathrm{B}}$, which is described as [37]

$$\begin{aligned} V_{\mathrm{rel}} &= V^{\mathrm{sym}}_{\mathrm{A}} \otimes V^{\mathrm{sym}}_{\mathrm{B}} \\ &= V_{j_{\mathrm{A}}+j_{\mathrm{B}}} \oplus V_{j_{\mathrm{A}}+j_{\mathrm{B}}-1} \oplus V_j \oplus \cdots V_{j_{\mathrm{A}}-j_{\mathrm{B}}}, \end{aligned} \tag{5}$$

where V_j is the subspace spanned by the basis $\{|j;m_j\rangle\rangle | -j \leqslant m_j \leqslant j\}$, where m_j is a quantum number (a half integer) given as $J_z|j;m_j\rangle\rangle = m_j|j;m_j\rangle\rangle$. These basis vectors satisfy $\boldsymbol{J}^2|j;m_j\rangle\rangle = j(j+1)|j;m_j\rangle\rangle$. The largest subspace $V_{j_{\mathrm{A}}+j_{\mathrm{B}}}$ is spanned by the fully symmetric spin states, which we just call a symmetric subspace, while the other subspaces we call asymmetric subspaces.

Finally, the eigenstates $|j;m_j\rangle\rangle$ in V_j are related to the basis vectors $|m_{\mathrm{A}}\rangle_{\mathrm{A}} \otimes |m_{\mathrm{B}}\rangle_{\mathrm{B}}$ ($\in V^{\mathrm{sym}}_{\mathrm{A}} \otimes V^{\mathrm{sym}}_{\mathrm{B}}$) via the Clebsch-Gordan coefficients $C^{jm}_{m_{\mathrm{A}}m_{\mathrm{B}}} = \langle\langle j;m_j|m_{\mathrm{A}}\rangle_{\mathrm{A}} \otimes |m_{\mathrm{B}}\rangle_{\mathrm{B}}$.

B. Dynamics and steady state

We will now investigate the spin relaxations in the double-domain system by solving the master equation (2) in the direct-sum spin space (5). As a first step, we take a spin configuration $N_{\mathrm{A}}{=}N$ ($\geqslant 1$) and $N_{\mathrm{B}} = 1$ with the initial state (3) as the simplest case. As the initial state has the populations only in the two subspaces $V_{j_{\mathrm{I}}}$ and $V_{j_{\mathrm{II}}}$ [$j_{\mathrm{I}} = (N+1)/2$, $j_{\mathrm{II}} = (N-1)/2$] and the $\boldsymbol{J}^2$ is a conserved observable, we only need these two subspaces to represent the dynamics. The relevant Hilbert subspace is given by

$$V_{\mathrm{rel}} = V_{j_{\mathrm{I}}} \oplus V_{j_{\mathrm{II}}}. \tag{6}$$

$V_{j_{\mathrm{I}}}$ is the symmetric subspace, whereas $V_{j_{\mathrm{II}}}$ is an asymmetric subspace. We illustrate the relevant space V_{rel} in a matrix form in Fig. 2. This property of the representation space is powerful both in analytical calculations and in numerical calculations.

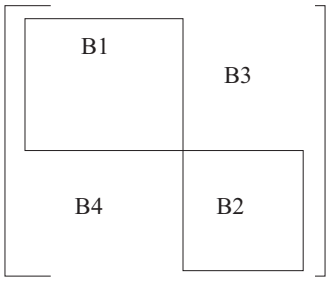

FIG. 2. The density matrix structure in the direct-sum spin space for $N_{\rm A} = N\ (\geqslant 1)$ and $N_{\rm B} = 1$. The diagonal blocks $\rm B_1$ and $\rm B_2$ are represented by basis vectors $\boldsymbol{e}_1 \sim \boldsymbol{e}_{N+2}$ and $\boldsymbol{e}_{N+3} \sim \boldsymbol{e}_{2(N+1)}$, respectively. Blocks $\rm B_3$ and $\rm B_4$ describe the off-diagonal parts.

We can solve the master equation (2) in the direct-sum spin space (6) by deriving the equations of motion for the matrix elements of the density matrix $\rho(t)$. First, we will label the spin states $|j_{\rm I(II)}; m_{\rm I(II)}\rangle\!\rangle$ as

$$\begin{aligned} \boldsymbol{e}_1 &= |j_{\rm I}; j_{\rm I}\rangle\!\rangle, \ldots \quad , \boldsymbol{e}_{N+2} = |j_{\rm I}; -j_{\rm I}\rangle\!\rangle, \\ \boldsymbol{e}_{N+3} &= |j_{\rm II}; j_{\rm II}\rangle\!\rangle, \ldots, \quad \boldsymbol{e}_{2(N+1)} = |j_{\rm II}; -j_{\rm II}\rangle\!\rangle. \end{aligned} \tag{7}$$

Second, we will label the rows and columns of the density matrix ρ using the basis vectors (7). The matrix elements are obtained as

$$\begin{aligned} \rho_{\alpha_{\rm I},\alpha'_{\rm I}} &= {}_{\rm I}\langle\!\langle j_{\rm I}; m^z_{\alpha_{\rm I}} | \rho | j_{\rm I}; m^z_{\alpha'_{\rm I}} \rangle\!\rangle_{\rm I}, \\ \rho_{\alpha_{\rm II},\alpha'_{\rm II}} &= {}_{\rm I}\langle\!\langle j_{\rm II}; m^z_{\alpha_{\rm II}} | \rho | j_{\rm II}; m^z_{\alpha'_{\rm II}} \rangle\!\rangle_{\rm I}, \\ \rho_{\alpha_{\rm I},\alpha_{\rm II}} &= {}_{\rm I}\langle\!\langle j_{\rm I}; m^z_{\alpha_{\rm I}} | \rho | j_{\rm II}; m^z_{\alpha_{\rm II}} \rangle\!\rangle_{\rm I}. \end{aligned} \tag{8}$$

Here the indices $\alpha_{\rm I}, \alpha'_{\rm I}$ run from 1 to $N+2$, whereas $\alpha_{\rm II}, \alpha'_{\rm II}$ run from $N+3$ to $2N+2$. The values $m^z_{\alpha_{\rm I}}$ and $m^z_{\alpha_{\rm II}}$ are the eigenvalues corresponding to the eigenstates $\boldsymbol{e}_{\alpha_{\rm I}}$ and $\boldsymbol{e}_{\alpha_{\rm II}}$ in Eq. (7), respectively. The state $|j_{\rm I(II)}; m^z_{\alpha_{\rm I(II)}}\rangle\!\rangle_{\rm I}$ is defined by $|j_{\rm I(II)}; m^z_{\alpha_{\rm I(II)}}\rangle\!\rangle_{\rm I} = \exp(i\omega J^z t)|j_{\rm I(II)}; m^z_{\alpha_{\rm I(II)}}\rangle\!\rangle$. As presented in Fig. 2, the representation of density matrix ρ in the direct-sum spin space is described in terms of four blocks: A block $\rm B_1$ is the symmetric part labeled by the basis vectors $\boldsymbol{e}_1 \sim \boldsymbol{e}_{N+2}$ and the matrix elements here are given by $\rho_{\alpha_{\rm I},\alpha'_{\rm I}}$ in Eq. (8). A block $\rm B_2$ is the asymmetric part labeled by $\boldsymbol{e}_{N+3} \sim \boldsymbol{e}_{2(N+1)}$. The corresponding matrix elements are $\rho_{\alpha_{\rm II},\alpha'_{\rm II}}$ in Eq. (8). Blocks $\rm B_3$ and $\rm B_4$ are the cross terms between the symmetric and asymmetric parts. The matrix elements in $\rm B_3$ are given by $\rho_{\alpha_{\rm I},\alpha_{\rm II}}$ in Eq. (8), and their Hermitian conjugates are equal to the matrix elements in block $\rm B_4$. Third, by multiplying $\langle\!\langle j_{\rm I(II)}; m^z_{\alpha_{\rm I(II)}}|$ to the left-hand side of Eq. (2) while $|j_{\rm I(II)}; m^z_{\alpha_{\rm I(II)}}\rangle\!\rangle$ is to the right-hand side of it, we have the equations of motion for the matrix elements

$$\begin{aligned} \dot{\rho}_{\alpha_{\rm I},\alpha'_{\rm I}} &= 2\gamma\left[\left(j_{\rm I} - m^z_{\alpha_{\rm I}}\right)\left(j_{\rm I} + m^z_{\alpha_{\rm I}} + 1\right)\left(j_{\rm I} - m^z_{\alpha'_{\rm I}}\right)\left(j_{\rm I} + m^z_{\alpha'_{\rm I}} + 1\right)\right]^{\frac{1}{2}} \rho_{\alpha_{\rm I}-1,\alpha'_{\rm I}-1} \\ &\quad - \gamma\left[\left(j_{\rm I} + m^z_{\alpha_{\rm I}}\right)\left(j_{\rm I} - m^z_{\alpha_{\rm I}} + 1\right) + \left(j_{\rm I} + m^z_{\alpha'_{\rm I}}\right)\left(j_{\rm I} - m^z_{\alpha'_{\rm I}} + 1\right)\right]\rho_{\alpha_{\rm I},\alpha'_{\rm I}}, \end{aligned} \tag{9}$$

$$\begin{aligned} \dot{\rho}_{\alpha_{\rm II},\alpha'_{\rm II}} &= 2\gamma\left[\left(j_{\rm II} - m^z_{\alpha_{\rm II}}\right)\left(j_{\rm II} + m^z_{\alpha_{\rm II}} + 1\right)\left(j_{\rm II} - m^z_{\alpha'_{\rm II}}\right)\left(j_{\rm II} + m^z_{\alpha'_{\rm II}} + 1\right)\right]^{\frac{1}{2}} \rho_{\alpha_{\rm II}-1,\alpha'_{\rm II}-1} \\ &\quad - \gamma\left[\left(j_{\rm II} + m^z_{\alpha_{\rm II}}\right)\left(j_{\rm II} - m^z_{\alpha_{\rm II}} + 1\right) + \left(j_{\rm II} + m^z_{\alpha'_{\rm II}}\right)\left(j_{\rm II} - m^z_{\alpha'_{\rm II}} + 1\right)\right]\rho_{\alpha_{\rm II},\alpha'_{\rm II}}, \end{aligned} \tag{10}$$

$$\begin{aligned} \dot{\rho}_{\alpha_{\rm I},\alpha_{\rm II}} &= 2\gamma\left[\left(j_{\rm I} - m^z_{\alpha_{\rm I}}\right)\left(j_{\rm I} + m^z_{\alpha_{\rm I}} + 1\right)\left(j_{\rm II} - m^z_{\alpha_{\rm II}}\right)\left(j_{\rm II} + m^z_{\alpha_{\rm II}} + 1\right)\right]^{\frac{1}{2}} \rho_{\alpha_{\rm I}-1,\alpha_{\rm II}-1} \\ &\quad - \gamma\left[\left(j_{\rm I} + m^z_{\alpha_{\rm I}}\right)\left(j_{\rm I} - m^z_{\alpha_{\rm I}} + 1\right) + \left(j_{\rm II} + m^z_{\alpha_{\rm II}}\right)\left(j_{\rm II} - m^z_{\alpha_{\rm II}} + 1\right)\right]\rho_{\alpha_{\rm I},\alpha_{\rm II}}. \end{aligned} \tag{11}$$

Equations (9), (10), and (11) are the equations of motion for the matrix elements in blocks $\rm B_1$, $\rm B_2$, and $\rm B_3$, respectively. The equations of motion for the matrix elements in block $\rm B_4$ are obtained by taking the Hermitian conjugate of Eq. (11). To derive the above equations we have used the relations $J^{\pm}J^{\mp} = \boldsymbol{J}^2 - (J^z)^2 \pm J^z$ and $J^{\pm}_a|j_a, m_a\rangle\!\rangle = \sqrt{j_a(j_a+1) - m_a(m_a \pm 1)}|j_a, m_a \pm 1\rangle\!\rangle$ with $a = \rm I, II$.

The initial state (3) for this case is given by

$$|{\rm is}\rangle\!\rangle = \left|\frac{N}{2}\right\rangle_{\rm A} \otimes \left|-\frac{1}{2}\right\rangle_{\rm B}. \tag{12}$$

Now by using the relations [38]

$$\begin{aligned} \left|j_{\rm I}; \frac{N-1}{2}\right\rangle\!\!\right\rangle &= \left(\frac{1}{N+1}\right)^{\frac{1}{2}}\left|\frac{N}{2}\right\rangle_{\rm A} \otimes \left|-\frac{1}{2}\right\rangle_{\rm B} + \left(\frac{N}{N+1}\right)^{\frac{1}{2}}\left|\frac{N-2}{2}\right\rangle_{\rm A} \otimes \left|\frac{1}{2}\right\rangle_{\rm B}, \\ \left|j_{\rm II}; \frac{N-1}{2}\right\rangle\!\!\right\rangle &= \left(\frac{N}{N+1}\right)^{\frac{1}{2}}\left|\frac{N}{2}\right\rangle_{\rm A} \otimes \left|-\frac{1}{2}\right\rangle_{\rm B} - \left(\frac{1}{N+1}\right)^{\frac{1}{2}}\left|\frac{N-2}{2}\right\rangle_{\rm A} \otimes \left|\frac{1}{2}\right\rangle_{\rm B}, \end{aligned} \tag{13}$$

the density matrix for the initial state (12) can be represented in the direct-sum spin space as

$$\begin{aligned} \rho_{\rm is}(N) &= \frac{1}{N+1}\left|j_{\rm I}; \frac{N-1}{2}\right\rangle\!\!\right\rangle\!\!\left\langle\!\!\left\langle j_{\rm I}; \frac{N-1}{2}\right| + \frac{N}{N+1}\left|j_{\rm II}, \frac{N-1}{2}\right\rangle\!\!\right\rangle\!\!\left\langle\!\!\left\langle j_{\rm II}; \frac{N-1}{2}\right| \\ &\quad + \frac{\sqrt{N}}{N+1}\left(\left|j_{\rm I}; \frac{N-1}{2}\right\rangle\!\!\right\rangle\!\!\left\langle\!\!\left\langle j_{\rm II}; \frac{N-1}{2}\right| + \left|j_{\rm II}; \frac{N-1}{2}\right\rangle\!\!\right\rangle\!\!\left\langle\!\!\left\langle j_{\rm I}; \frac{N-1}{2}\right|\right), \end{aligned} \tag{14}$$

or the more compact form,

$$[\rho_{\rm is}(N)]_{2,2}=\frac{1}{N+1},\quad [\rho_{\rm is}(N)]_{N+3,N+3}=\frac{N}{N+1},\quad [\rho_{\rm is}(N)]_{2,N+3}=[\rho_{\rm is}(N)]_{N+3,2}=\frac{\sqrt{N}}{N+1}, \tag{15}$$

with all the remaining elements equal to zero. We will solve the Eqs. (9)–(11) under the initial conditions (15). Due to the factors appearing as $j_{\rm I,II}$ and $m^z_{\alpha_{\rm I,II}}$ in Eqs. (9)–(11), we can describe the effective dynamics of the matrix elements by two damping rates enhanced by N. This reflects that the double-spin-domain system exhibits the collective decay induced by the common reservoir. In the real systems, there are some effects which break this collective decay, such as dephasing effects. Even if the dephasing effects were included, we still could observe this collective decay in this double-domain system as long as its timescales are comparable to those of the dephasing process [39].

To see the dynamics of the matrix elements visually and what is occurring, we solve Eqs. (9)–(11) for $N=1,2,3$, and 4. What we are particularly interested in is the dynamics of matrix elements which contributes to the relaxation of smaller spin $J^z_{\rm B}$, because as we see later, this shows the negative-temperature-state relaxation. Thus, we analyze the dynamics of all the diagonal components as well as the off-diagonal elements contributing to the expectation values of $J^z_{\rm B}$. For instance, in the case of $N=2$ the expectation $\langle J^z_{\rm B}\rangle$ is described by $\langle J^z_{\rm B}\rangle=\frac{1}{6}[4\sqrt{2}{\rm Re}(\rho_{2,5}+\rho_{3,6})+3\rho_{1,1}+\rho_{2,2}-\rho_{3,3}-3\rho_{4,4}-\rho_{5,5}+\rho_{6,6}]$. In Fig. 3, we present the time evolution of the diagonal components. The horizontal axis represents the dimensionless time defined by $\tilde{t}=\gamma t$. Figures 3(a), 3(c) 3(e), and 3(g) plot the dynamics of the diagonal elements in block $\rm B_1$, whereas Figs. 3(b), 3(d) 3(f), and 3(h) display those in block $\rm B_2$ for $N=1,2,3$, and 4, respectively. From these eight figures, what we see is that only the diagonal components $\rho_{N+2,N+2}$ and $\rho_{2N+2,2N+2}$, which are the end points of blocks $\rm B_1$ and $\rm B_2$, respectively, survive at the steady state. The matrix element $\rho_{N+2,N+2}$ converges to $1/(N+1)$ while $\rho_{2N+2,2N+2}$ to $N/(N+1)$. This indicates that in each block the upper components are going toward the end points with preserving the probability weight of the diagonal components given at the initial time. Denoting the density matrix for the steady state as $\rho_{\rm ss}(N)$, we see that in block $\rm B_1$ all the diagonal components except for the end point $\rho_{N+2,N+2}$ vanish such that $[\rho_{\rm is}(N)]_{2,2}=[\rho_{\rm ss}(N)]_{N+2,N+2}$. Similarly, in block $\rm B_2$ only the end point $\rho_{2N+2,2N+2}$ survives such that $[\rho_{\rm is}(N)]_{N+3,N+3}=[\rho_{\rm ss}(N)]_{2N+2,2N+2}$. In contrast, in Fig. 4 we have demonstrated the dynamics of off-diagonal components in block $\rm B_3$, which contributes to the expectations of $J^z_{\rm B}$. All these matrix elements vanish at the steady state. We have also presented the dynamics of the matrix elements $[\rho_{\rm ss}(N)]_{N+2,2N+2}$, which are the end point of block $\rm B_3$. It is zero for the entire time. This is because at first from Eq. (11), the equation of motion for $[\rho_{\rm ss}(N)]_{3,N+3}$ is represented by the linear differential equation with its initial value zero, which means that $[\rho_{\rm ss}(N)]_{3,N+3}$ is zero for the entire time. Then again from Eq. (11), $[\rho_{\rm ss}(N)]_{4,N+4},\ldots,[\rho_{\rm ss}(N)]_{N+1,2N+1}$ and $[\rho_{\rm ss}(N)]_{N+2,2N+2}$ are zero for any time by the same reason for $[\rho_{\rm ss}(N)]_{3,N+3}$. Thus, even $[\rho_{\rm ss}(N)]_{N+2,N+2}$ and $[\rho_{\rm ss}(N)]_{2N+2,2N+2}$ are finite, their cross components $[\rho_{\rm ss}(N)]_{N+2,2N+2}$ and $[\rho_{\rm ss}(N)]_{2N+2,N+2}$ vanish. By using the same argument, we can verify that all the other off-diagonal elements remain zero under the time evolution. As a result, the only terms which survive at the steady state are $[\rho_{\rm ss}(N)]_{N+2,N+2}$ and $[\rho_{\rm ss}(N)]_{2N+2,2N+2}$.

From the above analysis, we can establish (see Appendix for details) that for any N the density matrix for the steady state has the form

$$\rho_{\rm ss}(N)=\sum_{i={\rm I}}^{\rm II}p_i|j_i;-j_i\rangle\!\rangle\langle\!\langle j_i;-j_i|, \tag{16}$$

with $p_{\rm I}=1/(N+1)$, $p_{\rm II}=N/(N+1)$. The steady state (16) can be represented in the matrix form as

$$\rho_{\rm ss}(N)=\left(\begin{array}{ccc|ccc} 0 & & & & & \\ & 0 & & & & \\ & & \ddots & & & 0 \\ & & & p_{\rm I} & & \\ \hline & & & & 0 & \\ & & 0 & & & \ddots \\ & & & & & p_{\rm II} \end{array}\right). \tag{17}$$

Next, let us look at the structure of the steady state (16). The first terms represents the ground state of the total spin because in this state all the spins align downward. The probability weight to be in this state is given by $1/(N+1)$. The second term describes the asymmetric state and includes the effect inherent to the double-domain structure (3) with its probability weight $N/(N+1)$. This effect becomes stronger as N gets larger, leading to the unusual relaxation processes which cannot be realized in the single-spin-domain system.

The above argument can be extended to a finite temperature case. The steady-state density matrix becomes

$$\rho_{\rm ss}(N,\beta)=\sum_{i={\rm I}}^{\rm II}p_i\rho^i_{\rm ss}(N,\beta), \tag{18}$$

where

$$\rho^{\rm I(II)}_{\rm ss}(N,\beta)=\frac{\sum_{\alpha_{\rm I(II)}}e^{-\beta H_{\rm s}}\left|j_{\rm I(II)};m^z_{\alpha_{\rm I(II)}}\right\rangle\!\!\left\rangle\!\!\left\langle j_{\rm I(II)};m^z_{\alpha_{\rm I(II)}}\right|}{\sum_{\alpha_{\rm I(II)}}\left\langle j_{\rm I(II)};m^z_{\alpha_{\rm I(II)}}\right|e^{-\beta H_{\rm s}}\left|j_{\rm I(II)};m^z_{\alpha_{\rm I(II)}}\right\rangle}, \tag{19}$$

with $H_{\rm s}=\hbar\omega_{\rm s}(J^z_{\rm A}+J^z_{\rm B})$. The density matrix $\rho^{\rm I(II)}_{\rm ss}(N,\beta)$ describes the canonical ensemble of spin $J_{\rm I(II)}$. The total steady-state density matrix $\rho_{\rm ss}(N,\beta)$ is described as the sum of these two canonical ensembles with the initially given probability weights $p_{\rm I}$ and $p_{\rm II}$. It represents that the double-spin domain relaxes so that in each diagonal block the spin ($J_{\rm I}$ or $J_{\rm II}$) relaxes to the canonical ensemble described by Eq. (19) with preserving the initially given probability weight. The steady

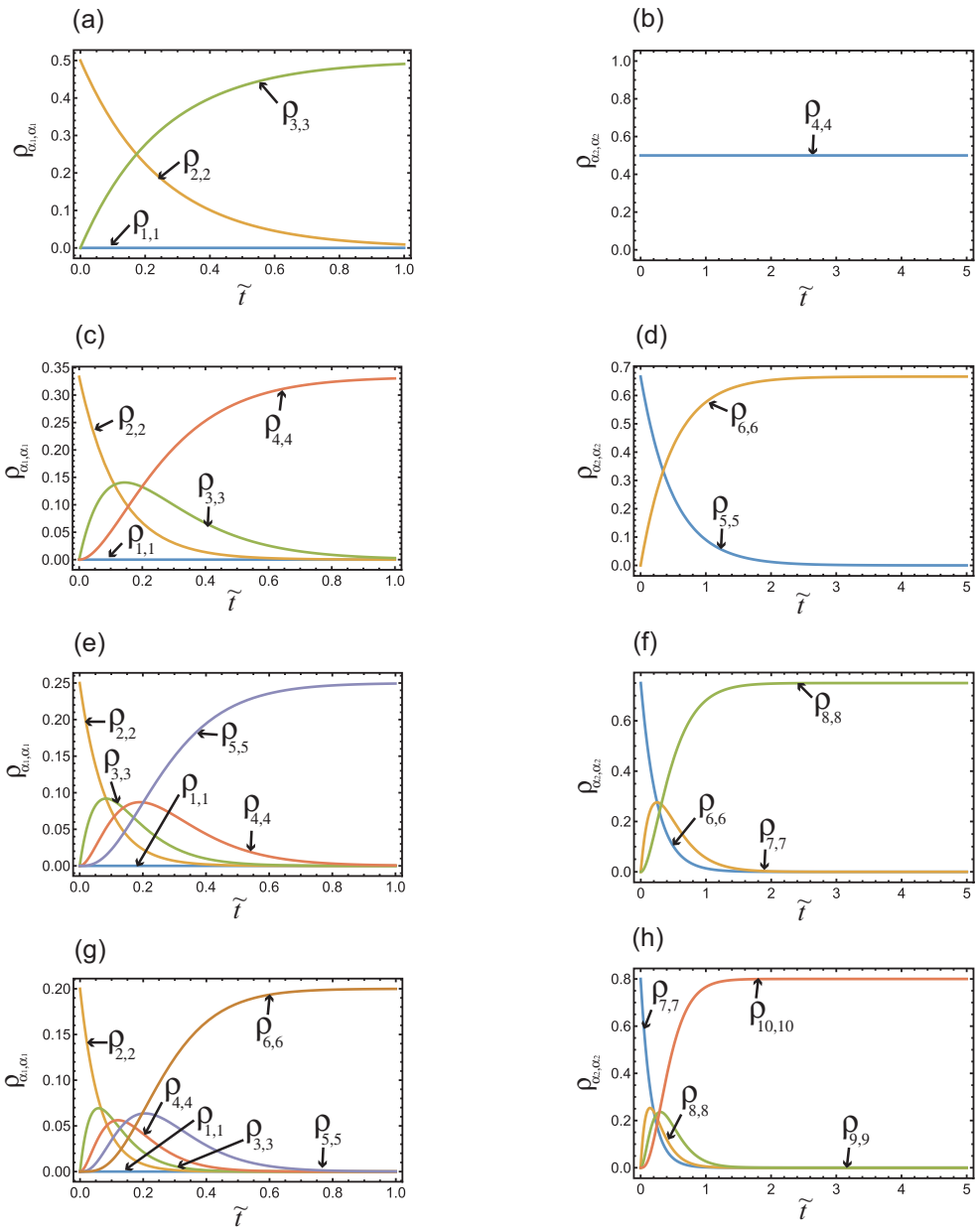

FIG. 3. The dynamics of the diagonal components of the density matrix in the direct-sum spin space. The horizontal axis denotes the dimensionless time $\tilde{t} = \gamma t$. (a, c, e, g) The dynamics of the diagonal elements in block B_1 and (b, d, f, h) those in block B_2 for $N = 1, 2, 3$, and 4, respectively. N_B is fixed to 1 for all figures. The only components which survive at the steady state are the end points of diagonal blocks: $\rho_{N+2,N+2}$ in block B_1 and $\rho_{2N+2,2N+2}$ in block B_2. $\rho_{N+2,N+2}$ converges to $1/(N+1)$, whereas $\rho_{2N+2,2N+2}$ converges to $N/(N+1)$.

state in Eq. (16) is reproduced by taking the limit $\beta \to \infty$ ($T \to 0$) in Eq. (18).

C. Negative-temperature-state relaxation

Having established the form of the steady state, we will analyze the spin polarization for each domain, especially the polarization for the small domain D_B. To calculate these quantities, we rewrite the steady state (16) in the tensor-product space representation using the relations [38]

$$
\begin{aligned}
|j_I; -j_I\rangle\rangle &= \left|-\frac{N}{2}\right\rangle_A \otimes \left|-\frac{1}{2}\right\rangle_B \\
|j_{II}; -j_{II}\rangle\rangle &= -\sqrt{\frac{N}{N+1}}\left|-\frac{N}{2}\right\rangle_A \otimes \left|\frac{1}{2}\right\rangle_B + \sqrt{\frac{1}{N+1}} \\
&\quad \times \left|-\frac{N-2}{2}\right\rangle_A \otimes \left|-\frac{1}{2}\right\rangle_B .
\end{aligned} \tag{20}
$$

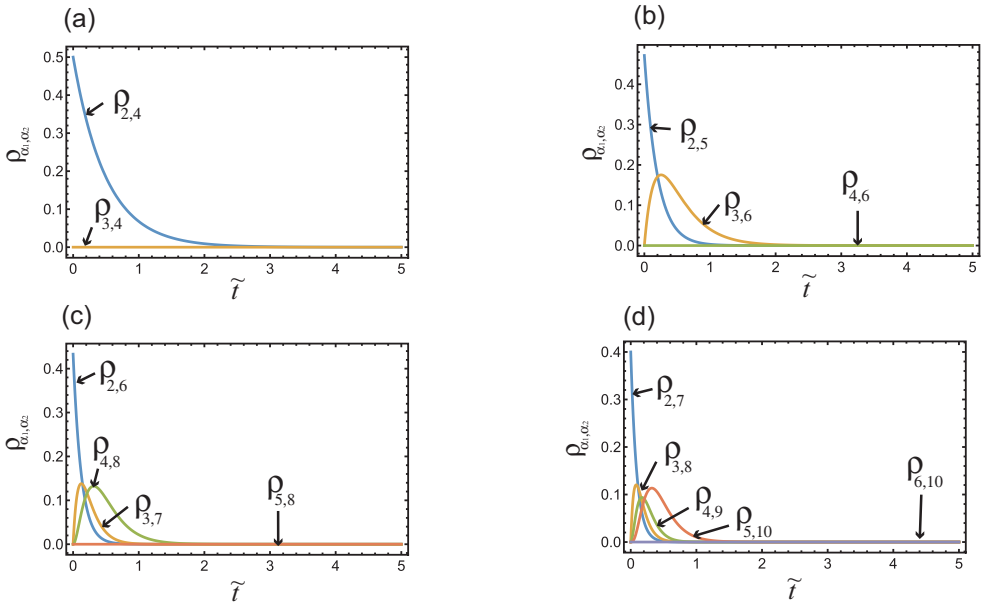

FIG. 4. The dynamics of the off-diagonal components of the density matrix in the direct-sum spin space. The horizontal axis describes the dimensionless time $\tilde{t} = \gamma t$. (a)–(d) The dynamics of the off-diagonal components in block B_3 for $N = 1, 2, 3$, and 4, respectively. All the components vanish at steady state.

The steady-state density matrix in the tensor-product spin space can be expressed as

$$\begin{aligned}\rho_{\rm ss}(N) = {} & \frac{1}{(N+1)}\left|-\frac{N}{2}\right\rangle_{\rm AA}\left\langle-\frac{N}{2}\right|\otimes\left|-\frac{1}{2}\right\rangle_{\rm BB}\left\langle-\frac{1}{2}\right| + \frac{N^2}{(N+1)^2}\left|-\frac{N}{2}\right\rangle_{\rm AA}\left\langle-\frac{N}{2}\right|\otimes\left|\frac{1}{2}\right\rangle_{\rm BB}\left\langle\frac{1}{2}\right| \\ & + \frac{N}{(N+1)^2}\left|-\frac{N-2}{2}\right\rangle_{\rm AA}\left\langle-\frac{N-2}{2}\right|\otimes\left|-\frac{1}{2}\right\rangle_{\rm BB}\left\langle-\frac{1}{2}\right| - \frac{N^{3/2}}{(N+1)^2}\left(\left|-\frac{N-2}{2}\right\rangle_{\rm AA}\right. \\ & \left.\times\left\langle-\frac{N}{2}\right|\otimes\left|-\frac{1}{2}\right\rangle_{\rm BB}\left\langle\frac{1}{2}\right| + \left|-\frac{N}{2}\right\rangle_{\rm AA}\left\langle-\frac{N-2}{2}\right|\otimes\left|\frac{1}{2}\right\rangle_{\rm BB}\left\langle-\frac{1}{2}\right|\right). \end{aligned} \tag{21}$$

From the above equation we obtain the spin polarization in the domain $D_{\rm A}$ at the steady state as

$$\left\langle J_{\rm A}^z\right\rangle_{\rm ss}(N) = {\rm Tr}\left[J_{\rm A}^z\rho_{\rm ss}(N)\right] = -\frac{N}{2}\frac{(N+1)^2-2}{(N+1)^2}, \tag{22}$$

while the spin polarization in the domain $D_{\rm B}$ is

$$\left\langle J_{\rm B}^z\right\rangle_{\rm ss}(N) = {\rm Tr}\left[J_{\rm B}^z\rho_{\rm ss}(N)\right] = \frac{(N-1)^2-2}{2(N+1)^2}. \tag{23}$$

We show the behavior of $\langle J_{\rm B}^z\rangle_{\rm ss}(N)$ in Fig. 5(a). We see that from $N = 3$, $J_{\rm B}^z$ becomes positive, which means that the spin population in the excited state is larger than that in the ground state, i.e., *the negative-temperature-state relaxation*. At $N \to \infty$, we have $\langle J_{\rm B}^z\rangle_{\rm ss} \to 1/2$, which means that $D_{\rm B}$ is completely excited while $\langle J_{\rm A}^z\rangle_{\rm ss} \to -N/2$, indicating that the larger spin domain $D_{\rm A}$ is in the ground state. The mechanism of the negative-temperature relaxation is clearly understood from the density matrix (16). The first term describes the ground state in the symmetric space. In this subspace, initially the spin state is prepared in the second highest energy level $\boldsymbol{e}_2$ in Eq. (7) and decays to the state $\boldsymbol{e}_{N+2}$ in Eq. (7). The second term in Eq. (16) represents the ground state in the asymmetric subspace. Initially, the spin state in this subspace is prepared in the highest energy level $\boldsymbol{e}_{N+3}$ in Eq. (7) and decays to the state $\boldsymbol{e}_{2N+2}$ in Eq. (7). This process gives the excitation to the double-spin domain so that $J_{\rm B}^z$ obtains the positive-polarization contribution. As mentioned previously, we see from Eq. (16) that the effect of the first term becomes smaller while that from the second term gets bigger as N increases. Therefore, $J_{\rm B}^z$ relaxes to the negative-temperature state and its effective temperature becomes lower as N increases.

Before ending this section, let us make a comparison between the negative-temperature state reported in the previous studies and the one presented in this paper. In [40,41], the negative-temperature state was realized using the interacting nuclear spins in a LiF crystal. Later, thermodynamic interpretations for these experimental results were given in [42,43]. (For other experimental examples and related theoretical works, see the references in [43].) The driving force to generate the negative-temperature state is the transient inversion of the direction of the external magnetic field. In this system, initially it is applied in a certain direction and the corresponding thermal equilibrium state is realized. Then the direction of the applied field is transiently switched to the opposite way from the initial one. As a result, a new thermal equilibrium state is generated. It is characterized by the negative temperature and is realized within the timescale in which

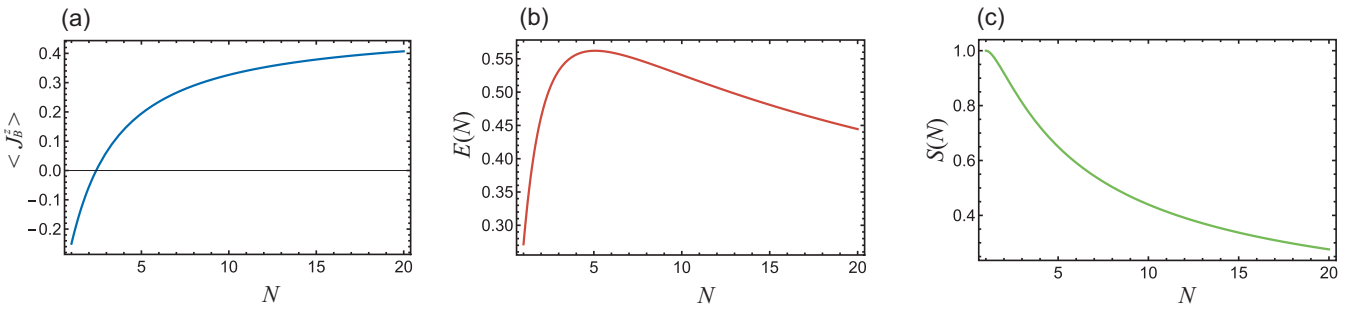

FIG. 5. (a) Plot of $\langle J_B^z \rangle$ as a function of N. The negative-temperature steady state starts to emerge from $N = 3$. (b) Plot of the amount of entanglement (logarithmic negativity) present as a function of N. It takes a maximum at $N = 5$. (c) Plot of the von Neumann entropy as a function of N. The steady state is maximally mixed at $N = 1$ and becomes a pure state at $N \to \infty$.

spin-spin interaction comes about. In contrast, the driving forces of our negative-temperature state are the unbalance between the two spin sizes and the common reservoir, which induces the collective spin decay. In real systems, both of these negative-temperature states do not survive for long due to couplings with other reservoirs. After a sufficiently long time has passed, spins relax to a different thermal equilibrium state described by a positive temperature.

D. Reservoir-assisted quantum entanglement

Next let us examine the quantum-entanglement creation between the two domains. From Eq. (21) we see that the terms in the first and second lines are written in a form $\sum_k w_k(\rho_k^A \otimes \rho_k^B)$ ($w_k \geqslant 0$, $\sum_k w_k = 1$), which is an expression for the density matrix of a quantum state in a separable state. The density matrix (21) is represented by this separable-state part and the additional terms which are written in the third line. Therefore, we readily see that the quantum entanglement is generated between the two domains at the steady state, namely, *the reservoir-assisted quantum entanglement*. The quantum entanglement generated by the common reservoir were also found in the different contexts, for instance, two-qubit systems [44–50], two harmonic-oscillator systems [51], and quantum entanglement in ionic, atomic, and nuclear ensemble systems [52–56]. (For other related topics of reservoir-assisted quantum entanglement, see, for instance, [57] and references therein.) Here we have found the reservoir-assisted quantum entanglement between the two spin domains as a consequence of the collective spin decay, where there is a small domain exhibiting the negative-temperature state.

Let us evaluate the quantum entanglement between the two spin domains. Here we use the logarithmic negativity [58,59]

$$E(\rho) = \log_2 \|\rho^{\Gamma_A}\|_1, \tag{24}$$

where Γ_A denotes the partial transposition with respect to subsystem A, and the trace norm $\|X\|_1$ is defined by $\|X\|_1 = \mathrm{Tr}|X| = \mathrm{Tr}\sqrt{X^\dagger X}$.

First, by taking the partial transpose to the density matrix (21), we have

$$\begin{aligned}(\rho_{\rm ss})^{\Gamma_{J_A}}(N) = {} & \frac{1}{(N+1)}\left|-\frac{N}{2}\right\rangle_{\rm AA}\left\langle-\frac{N}{2}\right| \otimes \left|-\frac{1}{2}\right\rangle_{\rm BB}\left\langle-\frac{1}{2}\right| + \frac{N^2}{(N+1)^2}\left|-\frac{N}{2}\right\rangle_{\rm AA}\left\langle-\frac{N}{2}\right| \otimes \left|\frac{1}{2}\right\rangle_{\rm BB}\left\langle\frac{1}{2}\right| \\ & + \frac{N}{(N+1)^2}\left|-\frac{N-2}{2}\right\rangle_{\rm AA}\left\langle-\frac{N-2}{2}\right| \otimes \left|-\frac{1}{2}\right\rangle_{\rm BB}\left\langle-\frac{1}{2}\right| - \frac{N^{3/2}}{(N+1)^2}\left(\left|-\frac{N-2}{2}\right\rangle_{\rm AA}\right. \\ & \left. \times \left\langle-\frac{N}{2}\right| \otimes \left|\frac{1}{2}\right\rangle_{\rm BB}\left\langle-\frac{1}{2}\right| + \left|-\frac{N}{2}\right\rangle_{\rm AA}\left\langle-\frac{N-2}{2}\right| \otimes \left|-\frac{1}{2}\right\rangle_{\rm BB}\left\langle\frac{1}{2}\right|\right).\end{aligned} \tag{25}$$

We note here that $(\rho_{\rm ss})^{\Gamma_{J_A}}(N) = (\rho_{\rm ss})^{\Gamma_{J_B}}(N)$. By deriving the eigenvalues of $\rho_{\rm ss}^{\Gamma_{J_A}}(N)$ [or $\rho_{\rm ss}^{\Gamma_{J_B}}(N)$], the logarithmic negativity for the matrix (25) is given by

$$E[(\rho_{\rm ss})^{\Gamma_{J_A}}(N)] = \log_2\left[\frac{\sqrt{4N^3 + (N+1)^2} + N^2 + N}{(N+1)^2}\right]. \tag{26}$$

We present the logarithmic negativity (26) in Fig. 5(b). It takes a maximum at $N = 5$ and its value is around 0.56. By comparing with the logarithmic negativities for the Bell states, which is equal to 1, we see that the two domains are quite entangled at this maximum point. The logarithmic negativity (26) becomes zero as $N \to \infty$. This can be easily understood from Eq. (21), because in this limit only the second term survives, which means that the steady state is in the separable state $|-\frac{N}{2}\rangle \otimes |\frac{1}{2}\rangle$.

Finally, let us discuss how pure the steady state (21) is. We evaluate its purity by the von Neumann entropy defined by

$$S[\rho_{\rm ss}(N)] = -\mathrm{Tr}[\rho_{\rm ss}(N)\log_2 \rho_{\rm ss}(N)]. \tag{27}$$

From the eigenvalues of the steady state (21), the von Neumann entropy becomes

$$S[\rho_{\rm ss}(N)] = -\frac{1}{N+1}\left(\log_2\frac{1}{N+1} + N\log_2\frac{N}{N+1}\right). \tag{28}$$

We plot this as a function of N in Fig. 5(c). The steady state (21) is maximally mixed at $N = 1$ and the entropy takes 1, and then it decreases as N increases. At $N \to \infty$, the entropy becomes zero, which is consistent with the above argument for the quantum entanglement because the steady state (21) becomes the pure state in this limit.

The negative-temperature-state relaxation (23) and the reservoir-assisted quantum entanglement (26) are the collective spin phenomena intrinsic to the double-domain system driven by the common reservoir. To see this clearly, let us compare the dynamics in a double-spin system, where each domain is individually coupled to a reservoir. Such dynamics is described by the Hamiltonian, e.g., Eq. (1), except the last interaction term is modified as $\hbar g_{\rm A}(J_{\rm A}^{+}R_{\rm A} + J_{\rm A}^{-}R_{\rm A}^{\dagger})/2 + \hbar g_{\rm B}(J_{\rm B}^{+}R_{\rm B} + J_{\rm B}^{-}R_{\rm B}^{\dagger})/2$. Each spin domain relaxes to its ground state, and the steady state is a separable state in terms of the ground state of the first domain and that of the second domain. Therefore, both the negative-temperature relaxation and the reservoir-assisted entanglement are not realized in this case.

IV. POTENTIAL IMPLEMENTATIONS

In this section, we present two candidate hybrid quantum systems to experimentally realize the spin collective phenomena described in Sec. III.

Quantum Hall system as a GaAs semiconductor. In this system, we can prepare a double spin domain of nuclei via dynamic nuclear polarization (DNP) [26–28]. First, the many-body electron-spin state is set into the filling factor 2/3 fractional quantum Hall (QH) regime. It consists of ferromagnetic and nonferromagnetic phases whose energies are degenerate. Then, by applying an ac electric current at about 100 nA, the scattering processes occur with some electrons flipping their spins while moving from the ferromagnetic part to the nonmagnetic part and vice versa. Subsequently, the nuclear spins get polarized dynamically and bidirectionally near the electric phase boundaries driven by the hyperfine interaction. As a result, the nuclear-double-spin domain is created as described by Eq. (3). Two nuclear domains are located in different electric phases (ferromagnetic or nonmagnetic phases). It has been recently measured in [28] that the nuclear polarization due to the DNP is about 26%. On the other hand, it was reported that the sizes of ferromagnetic and nonmagnetic regions are controllable by applying the gate bias voltage [34]. By preparing these two regions with the areas unbalanced, we can generate the unbalanced nuclear-double-spin domain. After the preparation of the initial state (double-spin domain) generated by the DNP, we couple the Nambu-Goldstone (NG) mode, which is going to act as a bosonic reservoir, to the nuclear-double-spin domain. At the Larmor frequency of nuclear spin which is around 10 MHz, the NG boson has a long wavelength which is much larger than the spin separation. Thus, the coupling between the NG mode and nuclear spins is spatially homogeneous [31]. Consequently, two nuclear-spin ensembles couple equivalently to the NG mode, and such a hybrid system is described by Eqs. (1) and (3). The NG-mode-induced nuclear-spin relaxation has been measured which featured the collective behavior [30] and was observed up to around 1 s. By preparing the large number of nuclear spins such that the collective decay is realized within 1 s, we observe our spin collective phenomena.

Nitrogen vacancy centers in a diamond coupled to a resonator. In this system, the electron-spin ensemble can be used for the spin domain while the resonator is used as the common bosonic reservoir. In [32], the superradiant decay of a single-electron-spin ensemble around 10^{16} was observed, which occurred in a few hundred nanoseconds. On the other hand, the coherent coupling between two-electron-spin ensembles in a quantum electrodynamic setup was realized in [33]. The initial state (3) can be prepared by applying an approximate π pulse to two spin ensembles. Further, the size of each spin ensemble can be controlled by tuning the concentration of the NV center. From these two experimental results and the approximated π pulse application for the initial state realization, we expect to observe our spin collective phenomena.

V. GENERALIZATION TO LARGER SPIN SYSTEMS

In this section, we will present the discussion for the spin configuration for $N_{\rm B} \geqslant 2$ (or the size of spin domain B larger than 1). First, we demonstrate the analysis in the case of $N_{\rm B} = 2$ by using the same argument which we did in Sec. III. Then by comparing the results for the steady state in the cases of $N_{\rm B} = 1, 2$, we will conjecture the steady-state solution for general $N_{\rm B}$.

The tensor-product spin space which describes the system dynamics is spanned by the eigenstates $|m_{\rm A}\rangle_{\rm A} \otimes |m_{\rm B}\rangle_{\rm B}$ with $m_{\rm A} = N/2, \ldots, -N/2$ and $m_{\rm B} = 1, 0, -1$. On the other hand, the corresponding direct-sum spin (symmetric-asymmetric) space has a structure

$$V_{\rm rel} = V_{j_1} \oplus V_{j_2} \oplus V_{j_3}, \tag{29}$$

where $j_1 = (N/2) + 1$, $j_2 = N/2$, and $j_3 = (N/2) - 1$. Again, V_{j_1}, V_{j_2}, and V_{j_3} are defined to accommodate the initial state. The basis vectors which span the Hilbert space (29) are

$$\begin{aligned} &\boldsymbol{e}_1 = |j_1; j_1\rangle\rangle, \ldots, \quad \boldsymbol{e}_{N+3} = |j_1; -j_1\rangle\rangle, \\ &\boldsymbol{e}_{N+4} = |j_2; j_2\rangle\rangle, \ldots, \quad \boldsymbol{e}_{2(N+2)} = |j_2; -j_2\rangle\rangle, \\ &\boldsymbol{e}_{2N+5} = |j_3; j_3\rangle\rangle, \ldots, \quad \boldsymbol{e}_{3(N+1)} = |j_3; -j_3\rangle\rangle. \end{aligned} \tag{30}$$

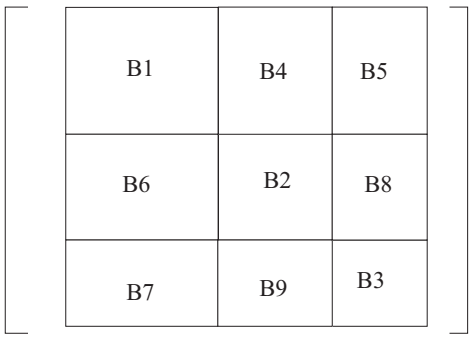

FIG. 6. The density matrix structure represented by the direct-sum spin space. There are nine sub-blocks and the diagonal parts are blocks B_1, B_2, and B_3.

The subspaces V_{j_1}, V_{j_2}, and V_{j_3} are spanned by the eigenstates $\boldsymbol{e}_1 \sim \boldsymbol{e}_{N+3}$, $\boldsymbol{e}_{N+4} \sim \boldsymbol{e}_{2(N+2)}$, and $\boldsymbol{e}_{2N+5} \sim \boldsymbol{e}_{3(N+1)}$, respectively. The subspace V_{j_1} is the symmetric subspace. The density matrix structure is represented by nine blocks as depicted in Fig. 6. Blocks B_1, B_2, and B_3 are the diagonal parts constructed by the eigenvectors $\boldsymbol{e}_1 \sim \boldsymbol{e}_{N+3}$, $\boldsymbol{e}_{N+4} \sim \boldsymbol{e}_{2(N+2)}$, and $\boldsymbol{e}_{2N+5} \sim \boldsymbol{e}_{3(N+1)}$, respectively. The other blocks $\mathrm{B}_4 \sim \mathrm{B}_9$ are the off-diagonal parts; for instance, in block B_4 the row is labeled by $\boldsymbol{e}_1 \sim \boldsymbol{e}_{N+2}$ whereas the column by $\boldsymbol{e}_{N+3} \sim \boldsymbol{e}_{2(N+2)}$.

Next, we derive the equations of motion for the matrix elements represented by the direct-sum spin space (29). From our master equation (2), we have

$$\dot{\rho}_{\alpha_i,\alpha_i'} = 2\gamma\left[\left(j_i - m_{\alpha_i}^z\right)\left(j_i + m_{\alpha_i}^z + 1\right)\left(j_i - m_{\alpha_i'}^z\right)\left(j_i + m_{\alpha_i'}^z + 1\right)\right]^{\frac{1}{2}}\rho_{\alpha_i-1,\alpha_i'-1} - \gamma\left[\left(j_i + m_{\alpha_i}^z\right)\left(j_i - m_{\alpha_i}^z + 1\right) + \left(j_i + m_{\alpha_i'}^z\right)\left(j_i - m_{\alpha_i'}^z + 1\right)\right]\rho_{\alpha_i,\alpha_i'}, \tag{31}$$

$$\dot{\rho}_{\alpha_i,\alpha_l} = 2\gamma\left[\left(j_i - m_{\alpha_i}^z\right)\left(j_i + m_{\alpha_i}^z + 1\right)\left(j_l - m_{\alpha_l}^z\right)\left(j_l + m_{\alpha_l}^z + 1\right)\right]^{\frac{1}{2}}\rho_{\alpha_i-1,\alpha_l-1} - \gamma\left[\left(j_i + m_{\alpha_i}^z\right)\left(j_i - m_{\alpha_i}^z + 1\right) + \left(j_l + m_{\alpha_l}^z\right)\left(j_l - m_{\alpha_l}^z + 1\right)\right]\rho_{\alpha_i,\alpha_l}, \quad (i \neq l) \tag{32}$$

with $i, l = 1, 2, 3$. The indices α_1, α_1' run from 1 to $N+3$, whereas α_2, α_2' runs from $N+4$ to $2(N+2)$, and α_3, α_3' from $2N+5$ to $3(N+1)$. The value $m_{\alpha_i}^z$ is the eigenvalue of the eigenstate $\boldsymbol{e}_{\alpha_i}$ with respect to J^z. We will solve the equations of motion (31) and (32) under the initial condition

$$|\mathrm{in}\rangle = \left|\frac{N}{2}\right\rangle_{\mathrm{A}} \otimes |-1\rangle_{\mathrm{B}}. \tag{33}$$

In the direct-sum spin space the initial state (33) is expressed as [38]

$$|\mathrm{in}\rangle = \sqrt{\frac{2}{(N+1)(N+2)}}\left|j_1; \frac{N}{2} - 1\right\rangle\!\!\right\rangle + \sqrt{\frac{2}{N+2}}\left|j_2; \frac{N}{2} - 1\right\rangle\!\!\right\rangle + \sqrt{\frac{N-1}{N+1}}\left|j_3; \frac{N}{2} - 1\right\rangle\!\!\right\rangle, \tag{34}$$

or

$$\begin{aligned}
&[\rho_{\mathrm{is}}(N)]_{3,3} = \frac{2}{(N+1)(N+2)}, \quad [\rho_{\mathrm{is}}(N)]_{N+5,N+5} = \frac{2}{N+2}, \quad [\rho_{\mathrm{is}}(N)]_{2N+5,2N+5} = \frac{N-1}{N+1},\\
&[\rho_{\mathrm{is}}(N)]_{3,N+5} = [\rho_{\mathrm{is}}(N)]_{N+5,3} = \frac{2}{N+2}\sqrt{\frac{1}{N+1}}, \quad [\rho_{\mathrm{is}}(N)]_{3,2N+5} = [\rho_{\mathrm{is}}(N)]_{2N+5,3} = \frac{1}{N+1}\sqrt{\frac{2(N-1)}{N+2}},\\
&[\rho_{\mathrm{is}}(N)]_{N+5,2N+5} = [\rho_{\mathrm{is}}(N)]_{2N+5,N+5} = \sqrt{\frac{2(N-1)}{(N+1)(N+2)}},
\end{aligned} \tag{35}$$

and the rest of components are zero. As in the case of $N_{\mathrm{A}} = N$, $N_{\mathrm{B}} = 1$, the two effective damping rates are enhanced as N increases, indicating the collective decay.

We derive the steady-state density matrix. First, for the matrix elements in block B_1, from the initial condition (35) we obtain $(\rho)_{1,1}(N,t) = (\rho)_{2,2}(N,t) = 0$. Then subsequently, we have

$$(\rho)_{3,3}(N,t) = \frac{2}{(N+1)(N+2)}\exp\left(-6N\gamma t\right). \tag{36}$$

At the steady state, $(\rho)_{3,3}$ is zero, and subsequently, we have $(\rho_{\mathrm{ss}})_{4,4} = \cdots = (\rho_{\mathrm{ss}})_{N+1,N+1} = 0$. Such an argument can be exactly applied to the diagonal matrix elements in blocks B_2 and B_3. Thus the only elements which survive at the steady state are the end points of blocks B_1, B_2, and B_3. We have $(\rho_{\mathrm{ss}})_{N+3,N+3} = p_1$, $(\rho_{\mathrm{ss}})_{2(N+2),2(N+2)} = p_2$, $(\rho_{\mathrm{ss}})_{3(N+1),3(N+1)} = p_3$, where p_1, p_2, p_3 are the finite constants satisfying $p_1 + p_2 + p_3 = 1$. For off-diagonal elements, whether they have finite values or not at the initial state, they become zero at the steady state. Therefore, by considering that the spin subspaces V_{j_1}, V_{j_2}, and V_{j_3} are orthogonal to each other, the constants p_1, p_2, p_3 must satisfy $p_1 = [\rho_{\mathrm{is}}(N)]_{3,3}$, $p_2 = [\rho_{\mathrm{is}}(N)]_{N+5,N+5}$, $p_3 = [\rho_{\mathrm{is}}(N)]_{2N+5,2N+5}$. As a result, the density matrix at steady state in the direct-sum space representation has a form

$$\rho_{\mathrm{ss}}(N) = \sum_{i=1}^{3} p_i \left|j_i; -j_i\right\rangle\!\!\right\rangle\!\!\left\langle\!\!\left\langle j_i; -j_i\right|, \tag{37}$$

where $p_1 = 2/(N+1)(N+2)$, $p_2 = 2/(N+2)$, $p_3 = (N-1)/(N+1)$. In a matrix form, the steady state (37) is represented as

$$\rho_{\rm ss}(N) = \left(\begin{array}{c|c|c} \begin{matrix} 0 & & \\ & \ddots & \\ & & p_1 \end{matrix} & \begin{matrix} 0 & & \\ & 0 & \\ & & 0 \end{matrix} & \begin{matrix} 0 & & \\ & 0 & \\ & & 0 \end{matrix} \\ \hline \begin{matrix} 0 & & \\ & 0 & \\ & & 0 \end{matrix} & \begin{matrix} 0 & & \\ & \ddots & \\ & & p_2 \end{matrix} & \begin{matrix} 0 & & \\ & 0 & \\ & & 0 \end{matrix} \\ \hline \begin{matrix} 0 & & \\ & 0 & \\ & & 0 \end{matrix} & \begin{matrix} 0 & & \\ & 0 & \\ & & 0 \end{matrix} & \begin{matrix} 0 & & \\ & \ddots & \\ & & p_3 \end{matrix} \end{array}\right). \tag{38}$$

The steady-state formula of the density matrix at finite temperature can be obtained by applying the similar analysis for the case of $N_{\rm A} = N$, $N_{\rm B} = 1$. It is given by

$$\rho_{\rm ss}(N,\beta) = \sum_{i=1}^{3} p_i \rho_{\rm ss}^i(N,\beta), \tag{39}$$

where

$$\rho_{\rm ss}^i(N,\beta) = \frac{\sum_{\alpha_i} e^{-\beta H_{\rm s}} \left| j_i; m_{\alpha_i}^z \right\rangle\!\!\left\rangle \left\langle\!\!\left\langle j_i; m_{\alpha_i}^z \right|}{\sum_{\alpha_i} \left\langle\!\!\left\langle j_i; m_{\alpha_i}^z \right| e^{-\beta H_{\rm s}} \left| j_i; m_{\alpha_i}^z \right\rangle\!\!\right\rangle}. \tag{40}$$

From the relations [38]

$$\begin{aligned} |j_1;-j_1\rangle\!\rangle &= \left|-\frac{N}{2}\right\rangle_{\rm A} \otimes |-1\rangle_{\rm B}, \quad |j_2;-j_2\rangle\!\rangle = -\sqrt{\frac{N}{N+2}}\left|-\frac{N}{2}\right\rangle_{\rm A} \otimes |0\rangle_{\rm B} + \sqrt{\frac{2}{N+2}}\left|-\frac{N}{2}+1\right\rangle_{\rm A} \otimes |-1\rangle_{\rm B}, \\ |j_3;-j_3\rangle\!\rangle &= \sqrt{\frac{N-1}{N+1}}\left|-\frac{N}{2}\right\rangle_{\rm A} \otimes |1\rangle_{\rm B} - \sqrt{\frac{2(N-1)}{N(N+1)}}\left|-\frac{N}{2}+1\right\rangle_{\rm A} \otimes |0\rangle_{\rm B} + \sqrt{\frac{2}{N(N+1)}}\left|-\frac{N}{2}+2\right\rangle_{\rm A} \otimes |-1\rangle_{\rm B}, \end{aligned} \tag{41}$$

the steady-state density matrix can be represented in the tensor-product space as

$$\begin{aligned} \rho_{\rm ss}(N) = {} & \frac{2}{(N+1)(N+2)}\left|-\frac{N}{2}\right\rangle_{\rm AA}\!\left\langle-\frac{N}{2}\right| \otimes |-1\rangle_{\rm BB}\langle -1| + \frac{2N}{(N+2)^2}\left|-\frac{N}{2}\right\rangle_{\rm AA}\!\left\langle-\frac{N}{2}\right| \otimes |0\rangle_{\rm BB}\langle 0| \\ & + \frac{4}{(N+2)^2}\left|-\frac{N}{2}+1\right\rangle_{\rm AA}\!\left\langle-\frac{N}{2}+1\right| \otimes |-1\rangle_{\rm BB}\langle -1| + \frac{(N-1)^2}{(N+1)^2}\left|-\frac{N}{2}\right\rangle_{\rm AA}\!\left\langle-\frac{N}{2}\right| \otimes |1\rangle_{\rm BB}\langle 1| \\ & + \frac{2(N-1)^2}{N(N+1)^2}\left|-\frac{N}{2}+1\right\rangle_{\rm AA}\!\left\langle-\frac{N}{2}+1\right| \otimes |0\rangle_{\rm BB}\langle 0| + \frac{2(N-1)}{N(N+1)^2}\left|-\frac{N}{2}+2\right\rangle_{\rm AA}\!\left\langle-\frac{N}{2}+2\right| \otimes |-1\rangle_{\rm BB}\langle -1| \\ & - \frac{2\sqrt{2N}}{(N+2)^2}\left(\left|-\frac{N}{2}\right\rangle_{\rm AA}\!\left\langle-\frac{N}{2}+1\right| \otimes |0\rangle_{\rm BB}\langle -1| + \left|-\frac{N}{2}+1\right\rangle_{\rm AA}\!\left\langle-\frac{N}{2}\right| \otimes |-1\rangle_{\rm BB}\langle 0|\right) \\ & - \frac{(N-1)^2}{(N+1)^2}\sqrt{\frac{2}{N}}\left(\left|-\frac{N}{2}\right\rangle_{\rm AA}\!\left\langle-\frac{N}{2}+1\right| \otimes |1\rangle_{\rm BB}\langle 0| + \left|-\frac{N}{2}+1\right\rangle_{\rm AA}\!\left\langle-\frac{N}{2}\right| \otimes |0\rangle_{\rm BB}\langle 1|\right) \\ & + \sqrt{\frac{2(N-1)^3}{N(N+1)^4}}\left(\left|-\frac{N}{2}\right\rangle_{\rm AA}\!\left\langle-\frac{N}{2}+2\right| \otimes |1\rangle_{\rm BB}\langle -1| + \left|-\frac{N}{2}+2\right\rangle_{\rm AA}\!\left\langle-\frac{N}{2}\right| \otimes |-1\rangle_{\rm BB}\langle 1|\right) \\ & - \frac{2\sqrt{(N-1)^3}}{N(N+1)^2}\left(\left|-\frac{N}{2}+1\right\rangle_{\rm AA}\!\left\langle-\frac{N}{2}+2\right| \otimes |0\rangle_{\rm BB}\langle -1| + \left|-\frac{N}{2}+2\right\rangle_{\rm AA}\!\left\langle-\frac{N}{2}+1\right| \otimes |-1\rangle_{\rm BB}\langle 0|\right). \end{aligned} \tag{42}$$

The polarizations of two domains are

$$\left\langle J_{\rm A}^z \right\rangle_{\rm ss}(N) = -\frac{N^5 + 5N^4 + 4N^3 - 16N^2 - 8N + 16}{2N(N+1)(N+2)^2}, \tag{43}$$

$$\left\langle J_{\rm B}^z \right\rangle_{\rm ss}(N) = \frac{N(N+1)(N^2-12)+8}{N(N+1)(N+2)^2}. \tag{44}$$

The negative-temperature-state relaxation emerges from $N = 4$. In the limit $N \to \infty$, the spin polarization in domain

D_A is $-N/2$ whereas the spin polarization in domain D_B becomes 1. Hence, the domain $D_{A(B)}$ is in the ground (excited) state. We will not calculate the logarithmic negativity (24) and just examine whether the quantum entanglement is generated or not between the two spin domains. The steady-state density matrix (42) consists of the separable-state part (the terms in the first, second, and third lines) plus the additional terms (from fourth to seventh lines). Thus, the quantum entanglement is generated between the spin domains.

Now let us predict the formula for the density matrix at the steady state in the direct-sum spin space representation for general N_B. By observing the steady-state density matrix structures (16) and (37) [note that the density matrices (16) and (37) are for $N_B = 1$ and 2, respectively), we see that in the direct-sum spin space the density matrix at the steady state has a structure such that only the end points in the diagonal blocks survive. To explain this in a little more detail, let us denote the diagonal blocks for the density matrix as B_1, B_2, ..., and B_{N_B+1}. Initially, in each block there is an element having finite value. Then, by analyzing the equations of motion for the matrix elements, at the steady state we may predict that only the end point in each block takes finite value and is equal to that of the element, which was initially finite. This is because the subspaces V_j $[j = (N_A + N_B)/2, \ldots, (N_A - N_B)/2]$, which construct the direct-sum spin space, are orthogonal to each other. Therefore, at the steady state the density matrix would have a structure

$$\rho_{ss}(N) = \sum_{i=1}^{N_B+1} P_i |j_i; -j_i\rangle\rangle\langle\langle j_i; -j_i|, \tag{45}$$

where $j_1 = (N_A + N_B)/2$, $j_2 = (N_A + N_B)/2 - 1, \ldots$ and $j_{N_B+1} = (N_A - N_B)/2$. The coefficients P_i satisfy the conditions $0 \leqslant P_i < 1$ and $\sum_{i=1}^{N_B+1} P_i = 1$. The matrix form of the steady state (45) is

$$\rho_{ss}(N) = \left(\begin{array}{c|c|c} 0 & & \\ \ddots & \cdots & 0 \\ & P_1 & \\ \hline \vdots & \ddots & \vdots \\ \hline & & 0 \\ 0 & \cdots & \ddots \\ & & P_{N_B+1} \end{array}\right). \tag{46}$$

The formula (45) is physically natural, because at zero temperature the total spin should relax so that the steady state must be described by the eigenstates whose eigenvalues take the minimum in the direct-sum spin subspaces which they belong to. Indeed, the formula (45) satisfies the master equation (2) as a steady-state solution. The steady-state formula at finite temperature would be obtained by replacing $|j_i; -j_i\rangle\rangle\langle\langle j_i; -j_i|$ with the density matrix representing the canonical ensemble of spin with its magnitude j_i. By using the Clebsch-Gordan coefficients and the description of the steady state (45) in the tensor-product subspace, we can discuss the two spin polarizations and whether the quantum entanglement is generated or not between the two domains.

VI. DISCUSSION AND CONCLUSIONS

In this paper, we have investigated the dynamics of the density matrix and its structure for the collective spin relaxation in the double-spin-domain system. In this system, the two spin domains couple equivalently to the common reservoir and the Hamiltonian is described by the total spin. At the initial time the spin ensemble in the first domain is in the excited state (all-up spin state) whereas the second spin ensemble is in the ground state (all-down spin state), with the first spin size much larger than the second one. The initial state does not have a full spin symmetry but is symmetric in each domain. Due to the angular-momentum conservation in the total system, the total system preserves the symmetry the initial state contains through the relaxation process. To analyze the spin relaxation process, the direct-sum spin space (direct sum of symmetric and asymmetric spaces) was more effective than the tensor-product representation. This representation allowed us to reduce the dimensionality of the relevant Hilbert space significantly, and hence it became possible for the system to be analytically tractable. For more complicated initial states, we may need to increase the dimensionality of the relevant Hilbert space; however, this method will be also effective and beneficial for both analytical and numerical calculations.

By analyzing the dynamics of the density-matrix elements in the direct-sum spin space, we have found that the density matrix for the collective spin relaxation had the following structure. The behavior of the density matrix shows that the populations in the symmetric space decays to its ground state, i.e., all spins are down, gradually losing the coherence between the symmetric and asymmetric subspaces. The behavior in the asymmetric space is the same, although some excitations in spins remains in its ground states. When we see this behavior in the composite picture (the tensor-product space), the second domain which started at its ground state (the spin down) will be relaxed to the excited state. The degree of the excitation is dependent on the difference of the spin domains in their size. For instance, in the case of the second spin number equal to 1, when the number of spins in the first domain is greater than 2, the spin in the second domain decays to populate more than 50% in the excited state, which indicates an effective negative temperature. As the first spin number becomes sufficiently larger, the second spin domain is (almost) completely in the excited state where all the spins are up.

The spin polarizations for both domains show the monotonic behaviors as functions of the first spin size in an opposite way. The quantum entanglement between the two domains exhibits the nonmonotonic behavior as a function of the first spin size. It is an increasing function when the first spin size is in the range from 1 to 5. Then when it becomes equal to 6 and starts to exceed, the quantum entanglement decreases monotonically and converges to zero. This behavior is consistent with the fact that when the first spin size is sufficiently large the steady state becomes separable, with the first spin domain being all down and the second spin domain all up. Correspondingly, the purity becomes 1 at the first spin number to infinity.

These collective phenomena never occur in the single-spin-domain system and must be the consequence of the

asymmetry of the spin state and the coupling to the common reservoir. The candidate hybrid quantum systems to observe these phenomena are the following: One is the GaAs semiconductor, where nuclear spins are coupling to the electron spins in the QH state through the hyperfine interaction. When we initially prepared the nuclear-double-spin domain having an antiparallel configuration induced by the DNP [26–28], by tuning the QH state such that the linear dispersing NG mode, as the bosonic reservoir emerges [29–31], we observe our collective phenomena. The second candidate is the electron-spin ensemble in the NV center in diamonds coupling to the superconducting resonator [33].

The interesting point of these two collective phenomena is that the characteristics of the steady state (the spin polarizations and the amount of quantum entanglement) are rather opposite to those at the initial time, although the steady states exhibit dependency to their initial states. This relaxation behavior can be interesting to apply to quantum state manipulation and quantum information processes. Usually, the decoherence induced by the reservoir is regarded as an obstacle to perform the quantum information processing, destroying the initial information of the system. In these systems, after the system completely relaxed, the system has some in-print of the information the system initially had. This property may be exploited to implement robust quantum state manipulation.

ACKNOWLEDGMENTS

Y.H. thanks Mohammad Hamzah Fauzi, John Nicholas Moore, and Yoshiro Hirayama for fruitful discussions on electron-nuclear-spin dynamics in a quantum Hall system as a GaAs semiconductor. This work was supported in part by a MEXT Grant-in-Aid for Scientific Research on Innovative Areas KAKENHI Grant No. JP15H05870 (Y.H., E.Y., and K.N.) and MEXT Grant-in-Aid for Scientific Research(S) KAKENHI Grant No. JP25220601 (E.Y. and K.N.).

APPENDIX: MATHEMATICAL PROOF OF EQ. (16)

In this section, we demonstrate the mathematical proof of Eq. (16) by dividing it into three parts. Part I is the discussion for the dynamics of the diagonal elements, whereas parts II and III are those for the off-diagonal elements.

Part I. Diagonal elements. First, let us look at the dynamics of diagonal elements $\rho_{\alpha_{\rm I},\alpha_{\rm I}}$ in block B_1 through the equation of motion, Eq. (9). For $\alpha_{\rm I}=1$, since the term $\rho_{\alpha_{\rm I}-1,\alpha_{\rm I}-1}$ does not exist, the equation of motion (9) is described solely by $\rho_{1,1}$ as a linear differential equation. Due to the initial condition (15), we readily obtain $\rho_{1,1}(t)=0$. Thus, Eq. (9) for $\alpha_{\rm I}=2$ becomes the linear equation which is simply described by $\rho_{2,2}$. From the initial condition (15), we obtain

$$(\rho)_{2,2}(N,t)=\frac{1}{N+1}\exp\left(-4N\gamma t\right). \tag{A1}$$

Next let us look at Eq. (9) for $\alpha_{\rm I}=3$, which is described by $\rho_{3,3}$ and $\rho_{2,2}$. Although we can solve this equation and obtained the solution $(\rho)_{3,3}(N,t)$ for any t, we argue the steady-state solution because this is our interest. At $t\to\infty$, both $(\dot{\rho})_{3,3}(N,t)$ and $(\rho)_{2,2}(N,t)$ vanish. Thus, we have $(\rho_{\rm ss})_{3,3}=0$. By applying the same argument to other components sequentially, we have $(\rho_{\rm ss})_{4,4}=\cdots=(\rho_{\rm ss})_{N+1,N+1}=0$. For $\alpha_{\rm I}=N+2$, which is the end point of block B_1, the right-hand side of the equation is described solely by $(\rho)_{N+1,N+1}$ because the second term vanishes. Therefore, we have $(\rho_{\rm ss})_{N+2,N+2}=a_{\rm I}=$ const. This argument can be exactly applied for the dynamics of matrix elements $\rho^{\rm s}_{\alpha_{\rm II},\alpha_{\rm II}}$ in block B_2 using the equation of motion, Eq. (10). We obtain $(\rho_{\rm ss})_{2N+2,2N+2}=a_{\rm II}=$ const, which is finite and the rest of the components are zero.

Part II. Off-diagonal elements 1. We discuss the dynamics of off-diagonal elements $\rho_{\alpha_{\rm I},\alpha_{\rm II}}$ in block B_3 using the equation of motion, Eq. (11). The elements we consider are $(\rho)_{2,N+3}(N,t)$ and related ones. The matrix element $(\rho)_{2,N+3}(N,t)$ is the only off-diagonal element having a finite value at initial time. We start from analyzing the dynamics of $(\rho)_{2,N+3}(N,t)$. Since $(\rho)_{1,N+2}(N,t)$ belongs to block B_1, the term $\rho_{\alpha_{\rm I}-1,\alpha_{\rm II}-1}$ in Eq. (11) vanishes. Thus, the equation of motion (11) for $\alpha_{\rm I}=2$, $\alpha_{\rm II}=N+3$ is solely described by $(\rho)_{2,N+3}(N,t)$. From the initial condition (15), it is solved as

$$(\rho)_{2,N+3}(N,t)=-\frac{\sqrt{N}}{N+1}\exp\left(-(3N-1)\gamma t\right). \tag{A2}$$

Next, what we do is we repeat exactly the same argument which we did in Part I. Here again, we just consider only the steady-state solutions. For $\alpha_{\rm I}=3$, $\alpha_{\rm II}=N+4$ the right-hand side of the equation of motion (11) is described by $(\rho^{\rm s})_{3,N+4}(N,t)$ and $(\rho)_{2,N+3}(N,t)$. From Eq. (A2), we see that the steady-state solution for $(\rho)_{2,N+3}(N,t)$ is zero. Therefore, the steady-state solution for $(\rho)_{3,N+4}(N,t)$ is also zero. We repeat this argument sequentially for $\alpha_{\rm I}=4,\alpha_{\rm II}=N+5,\ldots,\alpha_{\rm I}=N+1,\alpha_{\rm II}=2N+2$. Then we have $(\rho_{\rm ss})_{4,N+5}=\cdots=(\rho_{\rm ss})_{N+1,2N+2}=0$. As a result, the off-diagonal components for $\alpha_{\rm I}=3,4,\ldots,N+1,\alpha_{\rm II}=N+4,N+5,\ldots,2N+2$ vanish at the steady state. Such behaviors are consistent with the plots in Fig. 4.

Part III. Off-diagonal elements 2. In this part, we discuss the dynamics of off-diagonal elements $\rho_{\alpha_{\rm I},\alpha'_{\rm I}}$, $\rho_{\alpha_{\rm II},\alpha'_{\rm II}}$, and $\rho_{\alpha_{\rm I},\alpha_{\rm II}}$, which were not discussed in Part II. Since the arguments for $\rho_{\alpha_{\rm I},\alpha'_{\rm I}}$, $\rho_{\alpha_{\rm II},\alpha'_{\rm II}}$, and $\rho_{\alpha_{\rm I},\alpha_{\rm II}}$ become exactly the same, here we will present only the argument for $\rho_{\alpha_{\rm I},\alpha'_{\rm I}}$. These elements are the simplest cases to analyze the steady-state solution because from Eq. (15) all these components are zero at the initial state. First, we start with the dynamics of $\rho_{1,\alpha'_{\rm I}}$ ($\alpha'_{\rm I}>1$). From the equation of motion (9) and the initial condition (15), we have $(\rho)_{1,\alpha'_{\rm I}}(N,t)=0$. As we mentioned above, since all the components at initial time are zero, we can easily show that $(\rho)_{2,\alpha'_{\rm I}+1}(N,t)=(\rho)_{3,\alpha'_{\rm I}+2}(N,t)\cdots=(\rho)_{N+3-\alpha'_{\rm I},N+2}(N,t)=0$. Similarly, from the equations of motion, Eqs. (10) and (11), and the initial condition (15), all the matrix elements $\rho_{\alpha_{\rm II},\alpha'_{\rm II}}$ and $\rho_{\alpha_{\rm I},\alpha_{\rm II}}$ under consideration are zero. Therefore, all these off-diagonal elements vanish at steady state. This is consistent with the results shown in Fig. 4.

As a result, all the off-diagonal elements vanish at steady state. The only finite elements are $\rho_{N+2,N+2}$ and $\rho_{2N+2,2N+2}$. With taking account of the constraint $\mathrm{Tr}[\rho_{\rm ss}(N)]=1$, the natural choices for $[\rho_{\rm ss}(N)]_{N+2,N+2}=a_{\rm I}$ and $[\rho_{\rm ss}(N)]_{2N+2,2N+2}=a_{\rm II}$ are

$$a_{\rm I}=\frac{1}{N+1},\quad a_{\rm II}=\frac{N}{N+1}. \tag{A3}$$

This is because the symmetric subspace and asymmetric subspace are orthogonal to each other. There must be no spin population transfer between them. In other words, the probability weight for each spin subspace must be invariant under the time evolution. Indeed, this is what we see in Fig. 3. Consequently, we obtain the steady-state formula (16).

[1] A. Zeilinger, Rev. Mod. Phys. **71**, S288 (1999).
[2] E. A. Cornell and C. E. Wieman, Rev. Mod. Phys. **74**, 875 (2002).
[3] R. H. Dicke, Phys. Rev. **93**, 99 (1954).
[4] M. Wallquist, K. Hammerer, P. Rabl, M. Lukin, and P. Zoller, Phys. Scr. T **137**, 014001 (2009).
[5] Z.-L. Xiang, S. Ashhab, J. Q. You, and F. Nori, Rev. Mod. Phys. **85**, 623 (2013).
[6] G. Kurizki, P. Bertet, Y. Kubo, K. Mølmer, D. Petrosyan, P. Rabl, and J. Schmiedmayer, Proc. Natl. Acad. Sci. USA **112**, 3866 (2015).
[7] S. Putz, A. Angerer, D. O. Krimer, R. Glattauer, W. J. Munro, S. Rotter, J. Schmiedmayer, and J. Majer, Nat. Photonics **11**, 36 (2017).
[8] P. Forn-Díaz, J. J. García-Ripoll, B. Peropadre, J.-L. Orgiazzi, M. A. Yurtalan, R. Belyansky, C. M. Wilson, and A. Lupascu, Nat. Phys. **13**, 39 (2017).
[9] F. Yoshihara, T. Fuse, S. Ashhab, K. Kakuyanagi, S. Saito, and K. Semba, Nat. Phys. **13**, 44 (2017).
[10] F. Yoshihara, T. Fuse, Z. Ao, S. Ashhab, K. Kakuyanagi, S. Saito, T. Aoki, K. Koshino, and K. Semba, Phys. Rev. Lett. **120**, 183601 (2018).
[11] D. Leibfried, R. Blatt, C. Monroe, and D. Wineland, Rev. Mod. Phys. **75**, 281 (2003).
[12] J. M. Raimond, M. Brune, and S. Haroche, Rev. Mod. Phys. **73**, 565 (2001).
[13] H. Ritsch, P. Domokos, F. Brennecke, and T. Esslinger, Rev. Mod. Phys. **85**, 553 (2013).
[14] R. Hanson, L. P. Kouwenhoven, J. R. Petta, S. Tarucha, and L. M. K. Vandersypen, Rev. Mod. Phys. **79**, 1217 (2007).
[15] R. Schirhagl, K. Chang, M. Loretz, and C. L. Degen, Annu. Rev. Phys. Chem. **65**, 83 (2014).
[16] D. Lee, K. W. Lee, J. V. Cady, P. Ovartchaiyapong, and A. C. Bleszynski Jayich, J. Opt. **19**, 033001 (2017).
[17] M. Aspelmeyer, T. J. Kippenberg, and F. Marquardt, Rev. Mod. Phys. **86**, 1391 (2014).
[18] K. Nemoto and W. J. Munro, Phys. Lett. A **344**, 104 (2005).
[19] S. Putz, D. O. Krimer, R. Amsüss, A. Valookaran, T. Nöbauer, J. Schmiedmayer, S. Rotter, and J. Majer, Nat. Phys. **10**, 720 (2014).
[20] C. Grezes, Y. Kubo, B. Julsgaard, T. Umeda, J. Isoya, H. Sumiya, H. Abe, S. Onoda, T. Ohshima, K. Nakamura, I. Diniz, A. Auffeves, V. Jacques, J.-F. Roch, D. Vion, D. Esteve, K. Moelmer, and P. Bertet, C. R. Phys. **17**, 693 (2016).
[21] L.-M. Duan, M. D. Lukin, J. I. Cirac, and P. Zoller, Nature (London) **414**, 413 (2001).
[22] M. Gross and S. Haroche, Phys. Rep. **93**, 301 (1982).
[23] K. Cong, Q. Zhang, Y. Wang, G. T. Noe II, A. Belyanin, and J. Kono, J. Opt. Soc. Am. B **33**, C80 (2016).
[24] J. F. Poyatos, J. I. Cirac, and P. Zoller, Phys. Rev. Lett. **77**, 4728 (1996).
[25] S. Diehl, A. Micheli, A. Kantian, B. Kraus, H. P. Büchler, and P. Zoller, Nat. Phys. **4**, 878 (2008).
[26] M. H. Fauzi, S. Watanabe, N. Kumada, and Y. Hirayama, J. Korean Phys. Soc. **60**, 1676 (2012).
[27] M. H. Fauzi, S. Watanabe, and Y. Hirayama, Appl. Phys. Lett. **101**, 162105 (2012).
[28] S. Miyamoto, T. Hatano, S. Watanabe, and Y. Hirayama, arXiv:1605.06926.
[29] N. Kumada, K. Muraki, and Y. Hirayama, Science **313**, 329 (2006); Phys. Rev. Lett. **99**, 076805 (2007).
[30] M. H. Fauzi, S. Watanabe, and Y. Hirayama, Phys. Rev. B **90**, 235308 (2014).
[31] Y. Hama, M. H. Fauzi, K. Nemoto, Y. Hirayama, and Z. F. Ezawa, New. J. Phys. **18**, 023027 (2016).
[32] A. Angerer, K. Streltsov, T. Astner, S. Putz, H. Sumiya, S. Onoda, J. Isoya, W. J. Munro, K. Nemoto, J. Schmiedmayer, and J. Majer, Nat. Phys. (2018), doi: 10.1038/s41567-018-0269-7.
[33] T. Astner, S. Nevlacsil, N. Peterschofsky, A. Angerer, S. Rotter, S. Putz, J. Schmiedmayer, and J. Majer, Phys. Rev. Lett. **118**, 140502 (2017).
[34] J. N. Moore, J. Hayakawa, T. Mano, T. Noda, and G. Yusa, Phys. Rev. Lett. **118**, 076802 (2017).
[35] Y. Hama, W. J. Munro, and K. Nemoto, Phys. Rev. Lett. **120**, 060403 (2018).
[36] H. J. Carmichael, *Statistical Methods in Quantum Optics 1: Master Equations and Fokker-Planck Equations*, 2nd ed. (Springer, Berlin, 2002).
[37] J. J. Sakurai and J. Napolitano, *Modern Quantum Mechanics*, 2nd ed. (Addison-Wesley, San Francisco, 2011).
[38] V. Devanathan, *Angular Momentum Techniques in Quantum Mechanics* (Kluwer Academic, Boston, 1999).
[39] V. V. Temnov and U. Woggon, Phys. Rev. Lett. **95**, 243602 (2005).
[40] E. M. Purcell and R. V. Pound, Phys. Rev. **81**, 279 (1951).
[41] A. Abragam and W. G. Proctor, Phys. Rev. **106**, 160 (1957); **109**, 1441 (1958).
[42] N. F. Ramsey, Phys. Rev. **103**, 20 (1956).
[43] E. Abraham and O. Penrose, Phys. Rev. E **95**, 012125 (2017).
[44] M. S. Kim, J. Lee, D. Ahn, and P. L. Knight, Phys. Rev. A **65**, 040101(R) (2002).
[45] D. Braun, Phys. Rev. Lett. **89**, 277901 (2002).
[46] S. Oh and J. Kim, Phys. Rev. A **73**, 062306 (2006).
[47] L. D. Contreras-Pulido and R. Aguado, Phys. Rev. B **77**, 155420 (2008).
[48] S. Maniscalco, F. Francica, R. L. Zaffino, N. Lo Gullo, and F. Plastina, Phys. Rev. Lett. **100**, 090503 (2008); F. Francica, S. Maniscalco, J. Piilo, F. Plastina, and K.-A. Suominen, Phys. Rev. A **79**, 032310 (2009).
[49] Y. Lin, J. P. Gaebler, F. Reiter, T. R. Tan, R. Bowler, A. S. Sørensen, D. Leibfried, and D. J. Wineland, Nature (London) **504**, 415 (2013).
[50] S. Shankar, M. Hatridge, Z. Leghtas, K. M. Sliwa, A. Narla, U. Vool, S. M. Girvin, L. Frunzio, M. Mirrahimi, and M. H. Devoret, Nature (London) **504**, 419 (2013).

[51] F. Benatti and R. Floreanini, J. Phys. A **39**, 2689 (2006).
[52] S. Schneider and G. J. Milburn, Phys. Rev. A **65**, 042107 (2002).
[53] J. T. Barreiro, M. Müller, P. Schindler, D. Nigg, T. Monz, M. Chwalla, M. Hennrich, C. F. Roos, P. Zoller, and R. Blatt, Nature (London) **470**, 486 (2011).
[54] M. J. A. Schuetz, E. M. Kessler, L. M. K. Vandersypen, J. I. Cirac, and G. Giedke, Phys. Rev. Lett. **111**, 246802 (2013); Phys. Rev. B **89**, 195310 (2014).
[55] C. A. Muschik, E. S. Polzik, and J. I. Cirac, Phys. Rev. A **83**, 052312 (2011).
[56] H. Krauter, C. A. Muschik, K. Jensen, W. Wasilewski, J. M. Petersen, J. I. Cirac, and E. S. Polzik, Phys. Rev. Lett. **107**, 080503 (2011).
[57] L. Aolita, F. de Melo, and L. Davidovich, Rep. Prog. Phys. **78**, 042001 (2015).
[58] G. Vidal and R. F. Werner, Phys. Rev. A **65**, 032314 (2002).
[59] M. B. Plenio, Phys. Rev. Lett. **95**, 090503 (2005).